ATOP Dyes. Optimization of a Multifunctional Merocyanine Chromophore for High Refractive Index Modulation in Photorefractive Materials

Frank Würthner,*,† Sheng Yao,† Joachim Schilling,‡ Rüdiger Wortmann,§ Mesfin Redi-Abshiro,§ Erwin Mecher,⊥ Francisco Gallego-Gomez,⊥ and Klaus Meerholz⊥

Contribution from the Department of Organic Chemistry II, University of Ulm, Albert-Einstein-Allee 11, D-89081 Ulm, Germany, Department of Inorganic Chemistry, University of Ulm, Albert-Einstein-Allee 11, D-89081 Ulm, Germany, Department of Physical Chemistry, University of Kaiserslautern, Erwin Schrödinger-Strasse, D-67663 Kaiserslautern, Germany, and Department of Chemistry, Physical Chemistry, University of Munich, Butenandtstrasse 11, D-81377 München, Germany

Received June 27, 2000. Revised Manuscript Received January 5, 2001

Abstract: This paper reports synthesis, characterization and structural optimization of *a*mino-*t*hienyl-di*o*xocyano-*p*yridine (ATOP) chromophores toward a multifunctional amorphous material with unprecedented photorefractive performance. The structural (dynamic NMR, XRD) and electronic (UV/vis, electrooptical absorption, Kerr effect measurements) characterization of the ATOP chromophore revealed a cyanine-type π-conjugated system with an intense and narrow absorption band ($\epsilon_{max} = 140\,000$ L mol^{-1} cm^{-1}), high polarizability anisotropy ($\delta\alpha_0 = 55 \times 10^{-40}$ C V^{-1} m^2), and a large dipole moment (13 D). This combination of molecular electronic properties is a prerequisite for strong electrooptical response in photorefractive materials with low glass-transition temperature (T_g). Other important materials-related properties such as compatibility with the photoconducting poly(*N*-vinylcarbazole) (PVK) host matrix, low melting point, low T_g, and film-forming capabilities were optimized by variation of four different alkyl substituents attached to the ATOP core. A morphologically stable PVK-based composite containing 40 wt % of ATOP-3 showed an excellent photorefractive response characterized by a refractive index modulation of $\Delta n \approx 0.007$ and a gain coefficient of $\Gamma \approx 180$ cm^{-1} at a moderate electrical field strength of $E = 35$ V μm^{-1}. Even larger effects were observed with thin amorphous films consisting of the pure glass-forming dye ATOP-4 ($T_g = 16$ °C) and 1 wt % of the photosensitizer 2,4,7-trinitro-9-fluorenylidene-malononitrile (TNFM). This material showed complete internal diffraction at a field strength of only $E = 10$ V μm^{-1} and Δn reached 0.01 at only $E = 22$ V μm^{-1} without addition of any specific photoconductor.

Introduction

There has been considerable progress in the field of photorefractive (PR) organic materials during the last years.[1] Being observed for the first time in 1990 in an organic crystal[2] and in 1991 in polymers,[3] PR effects have meanwhile been realized in a vast number of organics, including polymer composites,[3−7] fully functionalized polymers,[8] low-molar-mass glasses,[9,10] liquid crystals,[11] and polymer-dispersed liquid crystals.[12] Many of these materials are already superior to well-known inorganic PR crystals with respect to refractive index modulation and gain coefficients. Promising applications of organic PR materials in optical data storage, real-time image processing, and phase conjugation have been demonstrated.[1,4] Widespread utilization of these materials in holography, however, requires a number of additional qualities such as larger refractive index modulation, faster holographic build-up time, increased hologram lifetime,

* To whom correspondence should be addressed.
†Department of Organic Chemistry II, University of Ulm.
‡Department of Inorganic Chemistry, University of Ulm.
§ Department of Physical Chemistry, University of Kaiserslautern.
⊥ Department of Chemistry, University of München.

(1) (a) Moerner, W. E.; Silence, S. M. *Chem. Rev.* **1994**, *94*, 127−155. (b) Zhang, Y.; Burzynski, R.; Ghosal, S.; Casstevens, M. K. *Adv. Mater.* **1996**, *8*, 111−125. (c) Moerner, W. E.; Grunnet-Jepsen, A.; Thompson, C. L. *Annu. Rev. Mater. Sci.* **1997**, *27*, 585−623. (d) Meerholz, K. *Angew. Chem.* **1997**, *109*, 981−985; *Angew. Chem., Int. Ed. Engl.* **1997**, *36*, 945−948. (e) Meerholz, K.; Kippelen, B.; Peyghambarian, N. In *Electrical and Optical Polymer Systems*; Wise, D. L., Wnek, G. E., Trantolo, D. J., Gresser, J. D., Cooper, T. M., Eds.; World Scientific: London, 1998; pp 571−632.

(2) Sutter, K., Günter, P. *J. Opt. Soc. Am. B* **1990**, *7*, 2274−22**.**

(3) Ducharme, S.; Scott, J. C.; Twieg, R. J.; Moerner, W. E. *Phys. Rev. Lett.* **1991**, *66*, 1846−1849.

(4) (a) Meerholz, K.; Volodin, B. L.; Sandalphon; Kippelen, B.; Peyghambarian, N. *Nature* **1994**, *371*, 497−500. (b) Zobel, O.; Eckl, M.; Strohriegl, P.; Haarer, D. *Adv. Mater*. **1995**, *7*, 911−914. (c) Cox, A. M.; Blackburn, D.; West, D. P.; King, T. A.; Wade, F. A.; Leigh, D. A. *Appl. Phys. Lett.* **1996**, *68*, 2801−2803. (d) Meerholz, K.; Bittner, R.; De Nardin, Y.; Bräuchle, C.; Hendrickx, E.; Volodin, B. L.; Kippelen, B.; Peyghambarian, N. *Adv. Mater.* **1997**, *9*, 1043−1046.

(5) Grunnet-Jepsen, A.; Thompson, C. L.; Twieg, R. J.; Moerner, W. E. *Appl. Phys. Lett*. **1997**, *70*, 1515−1517.

(6) (a) Kippelen, B.; Marder, S. R.; Hendrickx, E.; Maldano, J. L.; Guillernet, G.; Volodin, B. L.; Steele, D. D.; Enami, Y.; Sandalphon; Yao, Y. J.; Wang, J. F.; Röckel, H.; Erskine, L.; Peyghambarian, N. *Science* **1998**, *279*, 54−58. (b) Hendrickx, E.; Herlocker, J.; Maldonado, J. L.; Marder, S. R.; Kippelen, B.; Persoons, A.; Peyghambarian, N. *Appl. Phys. Lett.* **1998**, *72*, 1679−1681.

(7) (a) Würthner, F.; Wortmann, R.; Matschiner, R.; Lukaszuk, K.; Meerholz, K.; DeNardin, Y.; Bittner, R.; Bräuchle, C.; Sens, R. *Angew. Chem.* **1997**, *109*, 2933−2936; *Angew. Chem., Int. Ed. Engl.* **1997**, *36*, 2765−2768. (b) Meerholz, K.; DeNardin, Y.; Bittner, R.; Wortmann, R.; Würthner, F. *Appl. Phys. Lett.* **1998**, *73*, 4−6. (c) Würthner, F.; Legrand, C.; Mecher, E.; Meerholz, K.; Wortmann, R. *Polym. Mater. Sci. Eng*. **1999,** *80*, 252−254.

10.1021/ja002321g CCC: $20.00
Published on Web 03/21/2001

and improved morphological stability of the materials. In this paper, we concentrate on two aspects, refractive index modulation and morphological stability; we also discuss the tradeoff between these material properties and describe systematic strategies for their optimization.

The PR effect comprises a series of events taking place when two coherent laser beams interfere in a material that exhibits both *photoconductivity* and *electrooptical* (EO) *response*. In a first step charge carriers are generated in the bright regions of the interference pattern by photoexcitation of spectral sensitizers and charge transfer to the charge-transport agent (CTA). Subsequently, the mobile charges are transferred by the CTA from the bright to the dark regions by diffusion or, more effectively, by an electric-field-assisted drift process. The charges then get trapped and create a periodic space-charge distribution between bright and dark regions of the material. In a final step reorientation of dipolar EO chromophores occurs in the total electric field (external plus space-charge field), and a refractive index grating is produced. This multistep hologram formation process in photorefractive materials exhibits several unique features which are not achieved with other photoaddressable materials: (1) the refractive index gratings are out of phase with respect to the original light intensity pattern; (2) the writing process is fully reversible; and (3) only weak laser intensities are required. The phase shift between intensity and refractive index grating gives rise to energy exchange between the two writing beams ("two-beam coupling"), an effect characteristic of PR materials and of considerable interest for optical data processing.

Multicomponent organic materials seem to be well-suited to optimize the different optical and electrical functionalities due to their compositional flexibility. Currently, the most advanced organic PR materials are composites of two major components providing charge transport and EO response, small amounts of a photosensitizer for the given laser wavelength, and significant amounts of plastisizers. The latter are added to achieve low glass-transition temperatures (<25 °C), which facilitate device fabrication and allow for "orientational enhancement" (reorientation of dyes in the internal space-charge field).[13] Composites will probably also be the natural choice for industrial applications because they allow simple fine-tuning for applications with different demands. Organic CTAs are already well-established and successfully used in photocopiers, laser printers,[14,15] and, more recently, organic light-emitting devices.[16] EO chromophores, on the other hand, have been studied rather extensively in the field of nonlinear optics,[17] but hitherto no final candidates for technological applications have been identified. With regard to morphological properties, the composite should have the capability of forming amorphous films of high optical quality. Any microphase separation must be avoided because it will cause light scattering.

Eventually in 1996 the so-called "orientational enhancement effect"[13] in low-T_g polymeric PR materials was be consistently interpreted in terms of the *Kerr susceptibility* $\chi^{(3)}(-\omega;\omega,0,0)$, in contrast to the *Pockels susceptibility* $\chi^{(2)}(-\omega;\omega,0)$ in crystalline materials.[18] This allowed the derivation of a suitable figure-of-merit F^{Kerr} for the electronic properties of PR chromophores,

$$F^{\mathrm{Kerr}} = \frac{1}{M}\left[9\mu\cdot\beta + 2\mu^2\cdot\delta\alpha/(k_{\mathrm{B}}T)\right] \qquad (1)$$

where μ is the dipole moment, $\delta\alpha$ the anisotropy of the linear polarizability, β the second-order polarizability, k_{B} the Boltzmann constant, T the temperature, and M the molar mass.[18] Usually, the figure-of-merit is reported as $F_0{}^{\mathrm{Kerr}}$, where the subscript "0" indicates dispersion-free values at infinite wavelength ($\lambda \rightarrow \infty$).

On the basis of eq 1, clear guidelines for the most favorable chromophores could be developed. In a detailed study on two series of merocyanine chromophores covering the whole range of electronic structures from polyene-like to betaine-like, we could unambiguously confirm eq 1 and elucidate the various contributions.[19,20] It was shown that in contrast to permanently poled (e.g. crystalline or high-T_g polymeric) PR materials, where the nonlinearity only depends on the $\mu\cdot\beta$ Pockels term, PR effects in low-T_g materials are dominated by

(8) (a) Tamura, K.; Padias, A. B.; Hall, H. K., Jr.; Peyghambarian, N. *Appl. Phys. Lett.* **1992**, *60*, 1803−1805. (b) Kippelen, B.; Tamura, K.; Peyghambarian, N.; Padias, A. B.; Hall, H. K., Jr. *J. Appl. Phys.* **1993**, *74*, 3617−3619. (c) Kippelen, B.; Tamura, K.; Peyghambarian, N.; Padias, A. B.; Hall, H. K., Jr. *Phys. Rev. B* **1993**, *48*, 10710−10718. (d) Yu, L.; Chen, Y. M., Chan, W. K. *J. Phys. Chem.* **1995**, *99*, 2797−2802. (e) Yu, L.; Chan, W. K.; Peng, Z.; Gharavi, A. *Acc. Chem. Res.* **1996**, *29*, 13-21. (f) Peng, Z.; Gharavi, A. R.; Yu, L. *J. Am. Chem. Soc.* **1997**, *119*, 4622−4232. (g) Wang, L.; Wang, Q.; Yu, L. *Appl. Phys. Lett.* **1998**, *73*, 2546−2548. (h) Li, W.; Gharavi, A.; Wang, Q.; Yu, L. *Adv. Mater.* **1998**, *10*, 927−931. (i) Döbler, M.; Weder, C.; Neuenschwander, P.; Suter, U. W.; Follonier, S.; Bosshard, C.; Günter, P. *Macromolecules* **1998**, *31*, 6184−6189. (j) Schloter, S.; Hofmann, U.; Hoechstetter, K.; Bäuml, G.; Haarer, D. *J. Opt. Soc. Am. B* **1998**, *15*, 2560−2565. (k) Bratcher, M. S.; DeClue, M. S.; Grunnet-Jepsen, A.; Wright, D.; Smith, B. R.; Moerner, W. E.; Siegel, J. S. *J. Am Chem. Soc.* **1998**, *120*, 9680−9681. (l) Hattemer, E.; Zentel, R.; Mecher, E.; Meerholz, K. *Macromolecules* **2000**, *33*, 1972−1977.

(9) Lundquist, P. M.; Wortmann, R.; Geletneky, C.; Twieg, R. J.; Jurich, M.; Lee, V. Y.; Moylan, C. R.; Burland, D. M. *Science* **1996**, *274*, 1182−1185.

(10) (a) Li, W.; Gharavi, A.; Wang, Q.; Yu, L. *Adv. Mater.* **1998**, *10*, 927−931. (b) Wang, L.; Zhang, Y.; Wada, T.; Sasabe, H. *Appl. Phys. Lett.* **1996**, *69*, 728−730. (c) Wang, L.; Zhang, Y.; Wada, T.; Sasabe, H. *Appl. Phys. Lett.* **1997**, *70*, 2949−2951. (d) Grasruck, M.; Schreiber, A.; Hofmann, U.; Zilker, S.; Leopold, A.; Schloter, S.; Hohle, C.; Strohriegl, P.; Haarer, D. *Phys. Rev. B* **1999**, *60*, 16543−16548. (e) Hohle, C.; Hofmann, U.; Schloter, S.; Thelakkat, M.; Strohriegl, P.; Haarer, D.; Zilker, S. J. *J. Mater. Chem.* **1999**, *9*, 2205−2210.

(11) (a) Khoo, I. C.; Li, H.; Liang, Y. *Opt. Lett.* **1994**, *19*, 1723−1725. (b) Wiederrecht, G. P.; Yoon, B. A.; Wasielewski, M. R. *Science* **1996**, *270*, 1794−1797. (c) Wiederrecht, G. P.; Yoon, B. A.; Svec, W. A.; Wasielewski, M. R. *J. Am. Chem. Soc.* **1997**, *119*, 3358−2264.

(12) (a) Ono, H.; Kawatsuki, N. *Opt. Lett.* **1997**, *22*, 1144−1146. (b) Golemme, A.; Volodin, B. L.; Kippelen, B.; Peyghambarian, N. *Opt. Lett.* **1997**, *22*, 1226−1228. (c) Golemme, A.; Kippelen, B.; Peyghambarian, N. *Appl. Phys. Lett.* **1998**, *73*, 2408−2410.

(13) Moerner, W. E.; Silence, S. M.; Hache, F.; Bjorklund, G. C. *J. Opt. Soc. Am. B* **1994**, *11*, 320−330.

(14) Law, K.-Y. *Chem. Rev.* **1993**, *93*, 449−486.

(15) (a) Wiedemann, W. *Chem.-Z.* **1982**, 106, 275−287. (b) Gibson, H. W. *Polymer* **1984**, *25*, 3−27. (b) Strohriegl, P.; Grazulevicius, J. V. In *Handbook of Organic Conductive Molecules and Polymers*; Nalwa, H. S., Ed.; Wiley: Chichester, 1997; Vol. 1, pp 553−620.

(16) (a) Salbeck, J. *Ber. Bunsen-Ges. Phys. Chem.* **1996**, *100*, 1667−1677. (b) Friend, R. H.; Gymer, R. W.; Holmes, A. B.; Burroughes, J. H.; Marks, R. N.; Taliani, C.; Bradley, D. D. C.; Dos Santos, D. A.; Brédas, J. L.; Lögdlund, M.; Salaneck, W. R. *Nature* **1999**, *397*, 121−128. (c) Heeger, A. J. *Solid State Commun.* **1998**, *107*, 673−679.

(17) (a) Wolff, J. J.; Wortmann, R. *Adv. Phys. Org. Chem.* **1999**, *32*, 121−217. (b) Verbiest, T.; Houbrechts, S.; Kauranen, M.; Clays, K.; Persoons, A. *J. Mater. Chem.* **1997**, *7*, 2175−2189. (c) Kanis, D. R.; Ratner, M. A.; Marks, T. J. *Chem. Rev.* **1994**, *94*, 195−242. (d) Burland, D. M.; Miller, R. D.; Walsh, C. A. *Chem. Rev.* **1994**, *94*, 31−75.

(18) (a) Wortmann, R.; Poga, C.; Twieg, R. J.; Geletneky, C.; Moylan, C. R.; Lundquist, P. M.; DeVoe, R. G.; Cotts, P. M.; Horn, H.; Rice, J.; Burland, D. M. *J. Chem. Phys.* **1996**, *105*, 10637−10647. (b) Kippelen, B.; Meyers, F.; Peyghambarian, N.; Marder, S. *J. Am. Chem. Soc.* **1997,** *119*, 4559−4560.

(19) Wortmann, R.; Würthner, F.; Sautter, A.; Lukaszuk, K.; Matschiner, R.; Meerholz, K. *Proc. SPIE* **1998**, *3471*, 41−49.

(20) (a) Würthner, F.; Thalacker, C.; Matschiner, R.; Lukaszuk, K.; Wortmann, R. *Chem. Commun.* **1998**, 1739−1740. (b) Beckmann, S.; Etzbach, K.-H.; Krämer, P.; Lukaszuk, K.; Matschiner, R.; Schmidt, A. J.; Schuhmacher, P.; Sens, R.; Seybold, G.; Wortmann, R.; Würthner, F. *Adv. Mater.* **1999**, *11*, 536−541. (c) Wortmann, R.; Glania, C.; Krämer, P.; Lukaszuk, K.; Matschiner, R.; Twieg, R. J.; You, F. *Chem. Phys.* **1999**, *245*, 107−120.

Chart 1

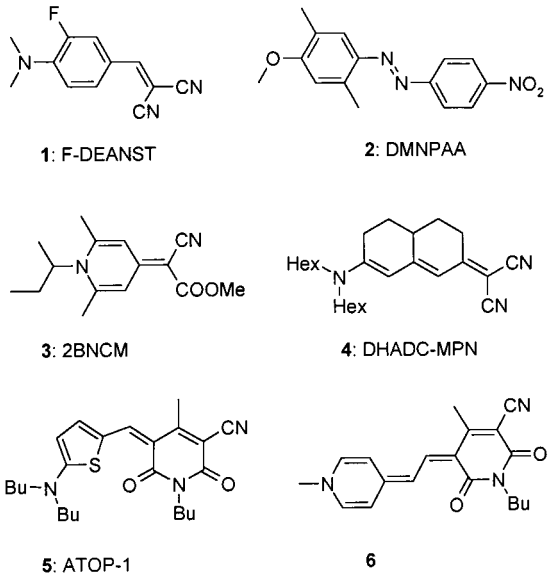

orientational birefringence related to the $\mu^2 \cdot \delta\alpha$ term. In view of the importance of the $\mu^2 \cdot \delta\alpha$ term the new dyes 2BNCM (**3**),[9] DHADC-MPN (**4**),[6] and ATOP-1 (**5**)[7] were synthesized (Chart 1). These dyes are all characterized by high $\delta\alpha$ but low β values and were successfully incorporated into highly promising PR materials. At least for DHADC-MPN and ATOP-1 based PR materials complete internal diffraction was achieved at lower dye concentrations than ever possible before with traditional EO chromophores such as F-DEANST (**1**) or DMNPAA (**2**). The highest F_0^{Kerr} value was reported for the highly dipolar merocyanine dye **6**, which exhibits a betainic character in the ground state.[19]

Although merocyanines in the cyanine limit (like ATOP-1, **5**) with equal contributions of the apolar (neutral) and the zwitterionic resonance structures exhibit the highest polarizability anisotropy $\delta\alpha$, the more betainic dyes such as **6** have the highest overall F_0^{Kerr} values because of their larger dipole moments. However, the beneficial effect of large dipole moments for dye orientation in electric fields is only given under ideal conditions in diluted solutions, while high dye concentrations are required to achieve the desired modulation efficiencies. Under these conditions serious problems due to dipolar aggregation and crystallization were noted.[21] Therefore, we decided to focus our further attempts to optimize the materials on the dyes with the highest $\delta\alpha$ values, i.e., the ATOP chromophore, which exhibit better solubility than dye **6** and reduced tendency for dipolar aggregation.

In the first part of this paper, we will characterize the structural and functional properties of ATOP rendering this chromophore superior to any other previously investigated dye within the field of organic PR materials. In the second part, we will show the important impact of alkyl substituents on the morphological and functional properties of the dyes and the PR composites. Finally, we will report the electrooptical and holographic characterization of a series of PVK-based PR composites with varying ATOP content (10−50 wt %). In one case (ATOP-4) PR devices were obtained from the bulk chromophore alone. The optimized materials display the strongest refractive index modulation ever reported in nonliquid-crystalline organic PR materials at low electrical field.

(21) Würthner, F.; Yao, S. *Angew. Chem., Int. Ed.* **2000**, *39*, 1978−1981.

Scheme 1

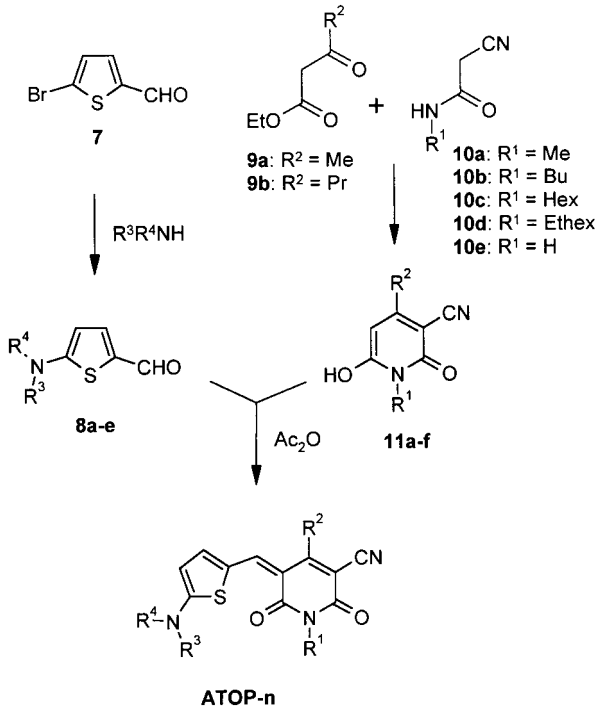

Table 1. ATOP Dyes Synthesized According to Scheme 1

dyes	starting materials	R^1	R^2	R^3	R^4	M (g/mol)
ATOP-1	**8c**, **11b**	Bu	Me	Bu	Bu	427
ATOP-2	**8a**, **11b**	Bu	Me	Me	Me	343
ATOP-3	**8b**, **11d**	2-Ethex[a]	Me	Et	Et	427
ATOP-4	**8c**, **11d**	2-Ethex[a]	Me	Bu	Bu	484
ATOP-5	**8a**, **11a**	Me	Me	Me	Me	301
ATOP-6	**8d**, **11b**	Bu	Me	Pip[b]		383
ATOP-7	**8e**, **11b**	Bu	Me	Et	Bu	400
ATOP-8	**8e**, **11c**	Hex	Me	Et	Bu	427
ATOP-9	**8e**, **11e**	Bu	Pr	Et	Bu	427
ATOP-10	**8c**, **11f**	H	Me	Bu	Bu	371

[a] 2-Ethylhexyl. [b] R^3, R^4 = Piperidine.

Results and Discussion

Synthesis. ATOP dyes were synthesized in high yields (57−87%) by condensation reactions of aldehydes **8a**−**e** and hydroxypyridones **11a**−**f** in acetic acid anhydride according to Scheme 1. The required aldehydes **8a**−**e** were obtained in yields of 50−70% from 2-bromo-5-formylthiophene **7**[22] and dialkylamines in nucleophilic displacement reactions and were typically used as crude materials (purity ≈ 90%).[23] Hydroxypyridines **11a**−**f** were obtained by condensation reactions of acyl acetates **9a,b** and cyanacetic acid amides **10a**−**e**.[24] Table 1 lists the compounds synthesized via this route along with their molar mass M. Note that according to eq 1, M influences the respective F_0^{Kerr} value.

Structural Properties of the ATOP Chromophore. Promising molecular structures for maximized PR response can be designed on the basis of eq 1. In this section we will characterize

(22) Weston, A. W.; Michaels, R. J., Jr. *J. Am. Chem. Soc.* **1950**, *72*, 1422−1423.

(23) (a) Nazarova, Z. N.; Pustarov, V. S. *Khim. Geterotsikl. Soedin.* **1969**, *5*, 586. A recently published method gave significantly lower yields: (b) Prim, D.; Kirsch, G.; Nicoud, J.-F. *Synlett* **1998**, 383−384.

(24) (a) Guareschi, J. *Ber. Dtsch. Chem. Ges. Board 4 (Referate, Patente, Nekrologe)*, **1896**, *29*, 654−656. (b) Bello, K. A. *Dyes Pigm.* **1995**, *28*, 83−90. (c) Katritzky, A. R.; Rachwal, S.; Smith, T. J. *Heterocycl. Chem.* **1995**, *32*, 1007−1010.

the structural properties of ATOP and show that this chromophore is indeed an excellent choice for this goal. Moreover, the structural investigation will reveal several geometrical features which distinguish ATOP from other merocyanine dyes (such as DHADC-MPN **4**) and which are considered to be important for high dye loading in PR composite materials.

(a) UV/Vis Absorption and Electrooptical Absorption Spectroscopy. Donor−acceptor substituted π-systems such as ATOP or the nonlinear optical (NLO) prototype molecule *p*-nitroaniline (pNA) usually exhibit a single intense charge-transfer transition (CT) in the UV/vis region which may be characterized by electrooptical absorption (EOA) spectroscopy[25,26] and analyzed according to eq 2

$$\epsilon^E(\phi,\tilde{\nu}) = \epsilon(\tilde{\nu})[1 + L(\phi,\tilde{\nu})E^2 + ...] \quad (2)$$

where ϵ^E is the absorption coefficient in the presence of the electric field E and L is a measure of the relative change of ϵ induced by E. L depends on the wavenumber $\tilde{\nu} = 1/\lambda$ as well as on the angle ϕ between the polarization vector of the incident light and the applied field. It has been shown that L may be interpreted in terms of the imaginary part of a third-order susceptibility, $\mathrm{Im}\{\chi^{(3)}(-\omega; \omega, 0,0)\}$.[26d]

Usually the EOA spectrum is recorded for two polarizations $\phi = 0°$ and 90°. A band shape analysis in terms of the optical absorption spectrum and its first derivative yields the ground-state dipole moment μ as well as the dipole difference between the ground state (g) and the excited state (a) $\Delta\mu$. Furthermore, knowledge of $\Delta\mu$ obtained from EOA allows one to estimate the static second-order polarizability β_0 and the anisotropy of the first-order polarizability $\delta\alpha_0$ of the dye within a two-level model:[18a,26b,27]

$$\delta\alpha_0 = 2\mu_{ag}{}^2\,\lambda_{ag}/(hc) \quad (3)$$

$$\beta_0 = 6\mu_{ag}{}^2\Delta\mu\lambda_{ag}{}^2/(hc)^2 \quad (4)$$

where the wavelength of maximum absorption λ_{ag} and the transition dipole moment μ_{ag} may be derived from the UV/vis spectrum.

Figure 1 shows the EOA spectrum of ATOP-1 taken in dioxane at a concentration of about 10^{-5} M. No aggregation is observed at this concentration (vide infra). The EOA spectrum of ATOP-1 is governed by two effects. The first is the *electrodichroic effect* caused by orientation of the chromophores in the externally applied electric field. For ATOP-1 there is strong *positive electrodichroism*, i.e., the absorption for parallel polarization ($\phi = 0°$) of the incident light field relative to the

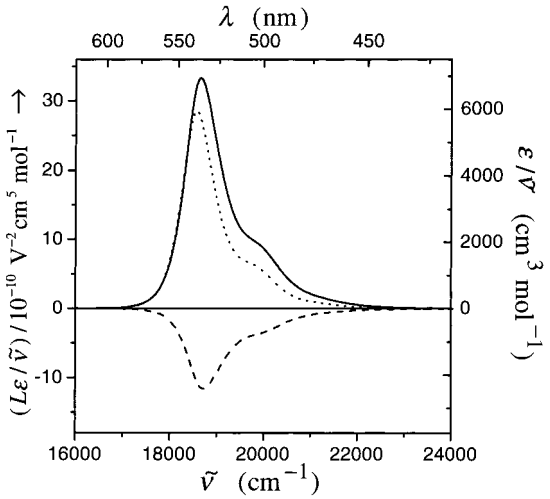

Figure 1. Optical (right scale; −) and electrooptical (left scale; $\phi = 0°$, ···; $\phi = 90°$, - - -) absorption spectra of ATOP-1 in dioxane at $T = 298$ K.

externally applied field increases while it decreases for the orthogonal polarization ($\phi = 90°$). This confirms that the ground-state dipole moment μ_g and the transition dipole moment μ_{ag} are essentially parallel and oriented along the conjugated chain. The second effect is the *band shift effect* (Stark effect) of the CT band in the electric field. It only occurs if the optical excitation is accompanied by a change of the dipole moment $\Delta\mu$. The EOA spectrum of ATOP-1 shows almost no shift of the spectrum, indicating a very small dipole difference $\Delta\mu$. The detailed band shape analysis yields $\mu = 44 \times 10^{-30}$ Cm (13 D), $\Delta\mu = 5.6 \times 10^{-30}$ Cm (1.7 D), $\mu_{ag} = 31 \times 10^{-30}$ Cm (9.3 D), and $\lambda_{ag} = 536$ nm, respectively (in dioxane at $T = 298$ K).

In addition, UV/vis spectra were recorded in solvents of different polarity. As expected from the EOA result $\Delta\mu \approx 0$, solvatochromism[28] of ATOP-1 was negligibly small, i.e., λ_{ag} was found to be almost independent of the solvent even for very different polarities: 531 (hexane), 532 (methanol), 535 (ether), 536 (dioxane), 536 (DMF), 538 (CCl_4), and 541 nm (CH_2Cl_2). Also the molar decadic absorption coefficient at the absorption maximum (ϵ_{max}) and the transition dipole moment μ_{ag} showed only little dependence on the solvent and ranged between 135 000 L mol^{-1} cm^{-1} in methanol and 150 000 L mol^{-1} cm^{-1} in CH_2Cl_2. For all solvents studied, the narrow (half width $\Delta\tilde{\nu}_{1/2} \approx 900$ cm^{-1}) and intense cyanine-like transition is preserved. This is advantageous for PR applications because laser wavelengths close to λ_{ag} may be used with such chromophores without absorption problems often encountered with the broad bands of traditional NLO dyes (cp. Figure 5 below). In this way one can take advantage of the considerable dispersion enhancement near the absorption edge.

With the experimental results for λ_{ag}, μ_{ag}, μ, and $\Delta\mu$ it is possible to estimate the linear and nonlinear polarizabilities as well as the figure-of-merit F_0^{Kerr} of ATOP-1 according to eqs 1−4. The results are $\delta\alpha_0 = 52 \times 10^{-40}$ C V^{-1} m^2, $\beta_0 = 23 \times 10^{-50}$ C V^{-2} m^3, and $F_0^{Kerr} = 1.40 \times 10^{-74}$ C^2 V^{-2} m^4

(25) (a) Liptay, W. In *Excited States, Vol. 1. Dipole Moments and Polarizabilities of Molecules in Excited Electronic States*; Lim, E. C., Ed.; Academic Press: New York, 1974; pp 129−229. (b) Wortmann, R.; Elich, K.; Lebus, S.; Liptay, W.; Borowicz, P.; Grabowska, A. *J. Phys. Chem.* **1992**, *96*, 9724−9730. (c) Bublitz, G. U.; Boxer, S. G. *Annu. Rev. Phys. Chem.* **1997**, *48*, 213−242. (d) Wolff, J. J.; Wortmann, R. *Adv. Phys. Org. Chem.* **1999**, *32*, 121−217.

(26) (a) Würthner, F.; Effenberger, F.; Wortmann, R.; Krämer, P. *Chem. Phys.* **1993**, *173*, 305−314. (b) Wortmann, R.; Krämer, P.; Glania,C.; Lebus, S.; Detzer, N. *Chem. Phys*. **1993**, *173*, 99−108. (c) Blanchard-Desce, M.; Wortmann, R.; Lebus, S.; Lehn, J.-M.; Krämer, P. *Chem. Phys. Lett*. **1995**, *243*, 526−532. (d) Blanchard-Desce, M.; Alain, V.; Midrier, L.; Wortmann, R.; Lebus, S.; Glania, C.; Krämer, P.; Fort, A.; Muller, J.; Barzoukas, M. *J. Photochem. Photobiol*. **1997**, *105*, 115−121. (e) Blanchard-Desce, M.; Alain, V.; Bedworth, P. V.; Marder, S. R.; Fort, A.; Runser, C.; Barzoukas, M.; Lebus, S.; Wortmann, R. *Chem. Eur. J*. **1997**, *3*, 1091−1104. (f) Steybe, F.; Effenberger, F.; Beckmann, S.; Krämer, P.; Glania, C.; Wortmann, R. *Chem. Phys.* **1997**, *219*, 317−331. (g) Bublitz, G. U.; Ortiz, R.; Runser, C.; Fort, A.; Barzoukas, M.; Marder, S. R.; Boxer, S. G. *J. Am. Chem. Soc.* **1997**, *119*, 2311−2312.

(27) Oudar, J. L.; Chemla, D. S. *J. Chem. Phys.* **1977**, *66*, 2664−2668.

(28) (a) Liptay, W. *Angew. Chem.* **1969**, *81*, 195−206; *Angew. Chem., Int. Ed. Engl.* **1969**, *8*, 177. (b) Liptay, W. *Z. Naturforsch.* **1965**, *20a*, 1441−1471.

(29) The structural and dipolar properties of the ATOP chromophore are reproduced fairly well by AM1 calculations which are in accordance with the crystal structure of ATOP-10 and measured dipole moments.

(30) (a) Jackman, L. M.; Cotton, F. A., Eds. *Dynamic Nuclear Magnetic Resonance Spectroscopy*; Academic Press: New York, 1975. (b) Kessler, H. *Angew. Chem.* **1970**, *82*, 237−253. (c) Stewart, W. E.; Sidall, T. H., III *Chem. Rev.* **1970**, *70*, 517−551.

mol kg^{-1}, respectively.[7] The value of the anisotropy of the linear polarizability was additionally confirmed by an independent Kerr effect measurement to be $\delta\alpha(-\omega;\ \omega) = 316 \times 10^{-40}$ C V^{-1} m^2 at the wavelength $\lambda = 589$ nm. Application of the two-level dispersion correction yields $\delta\alpha_0 = 55 \times 10^{-40}$ C V^{-1} for the static value in excellent agreement with the EOA result. In view of the similar molecular structure and the almost identical UV/vis absorption observed for all ATOP dyes we may assume equal values of μ, $\delta\alpha_0$, and β_0 for the dyes of this study, ATOP-1 to ATOP-10. However, differences in the figure-of-merit F_0^{Kerr} ranging from 1.24×10^{-74} C^2 V^{-2} m^4 mol kg^{-1} (ATOP-4) to 1.99×10^{-74} C^2 V^{-2} m^4 mol kg^{-1} (ATOP-5) result from the different molar masses (Table 1).

The electric properties of the dipolar ATOP dyes may be analyzed in terms of a simple CT model, which describes the ground and excited state as linear combinations of the neutral and zwitterionic resonance structures based on a resonance parameter c^2.[18a,20] Within this crude model donor−acceptor substituted π-conjugated chain molecules may be classified from polyene-type ($c^2 \approx 0$) over neutrocyanines ("cyanine limit", $c^2 \approx 0.5$) to betaine-type systems ($c^2 \approx 1$). A second parameter of this model is the maximal hypothetical dipole change $\Delta\mu_{\max}$, i.e., the difference of the dipole moments of the neutral and the zwitterionic resonance structure.[18a,20] Since this difference is proportional to the charge separation distance, $\Delta\mu_{\max}$ can be regarded as a measure of the effective CT length of the donor−acceptor system. The model parameters c^2 and $\Delta\mu_{\max}$ can be determined from the values of the transition dipole moment and the dipole difference according to

$$c^2 = {}^1/_2[1 - \Delta\mu(4\mu_{\mathrm{ag}}{}^2 + \Delta\mu^2)^{-1/2}] \quad (5)$$

$$\Delta\mu_{\max} = \Delta\mu/(1 - 2\,c^2) \quad (6)$$

For ATOP-1 the resonance parameter is found to be $c^2 = 0.46$ in dioxane solution, which indicates a structure close to the cyanine limit. The maximum dipole difference is found to be $\Delta\mu_{\max} = 62 \times 10^{-30}$ Cm (19 D), which corresponds to an effective CT length of 0.39 nm (~36% of the length of the π-conjugated system).

We further analyzed the HOMO and LUMO as well as the transition and dipole difference densities involved in the low-lying CT band of ATOP-1 (Figure 2b). These molecular properties were calculated with the CNDO/S method for AM1 optimized geometry.[29] The MO calculations reveal a unique electronic structure of the HOMO and LUMO where the number of nodes is *minimized in the transition densities* but *maximized in the difference density*. As a consequence, the magnitude of the transition dipole is almost maximized for the given topology, while the dipole difference is close to zero. This general tradeoff between μ_{ag} and $\Delta\mu$ has been discussed recently for a two-center CT system.[26d] The comparison with a similar calculation of the cyanine model chromophore shown in Scheme 2 reveals a close correspondence of the HOMO/LUMO structure with ATOP and supports the classification of ATOP as being close to the cyanine limit (Figure 2a).

(b) NMR Spectroscopy. The results on the cyanine-like electronic structure of the ATOP chromophore suggest mean bond orders of 1.5 for each carbon−carbon bond of the conjugated chain. However, deviations from this mean value might be expected for the individual bonds because the conjugated chain is partly embedded into heterocyclic units, i.e., the thiophene and the pyridone rings. Nevertheless, a high contribution of zwitterionic structures should result in restricted rotation also around those bonds, which are not fixed in a ring

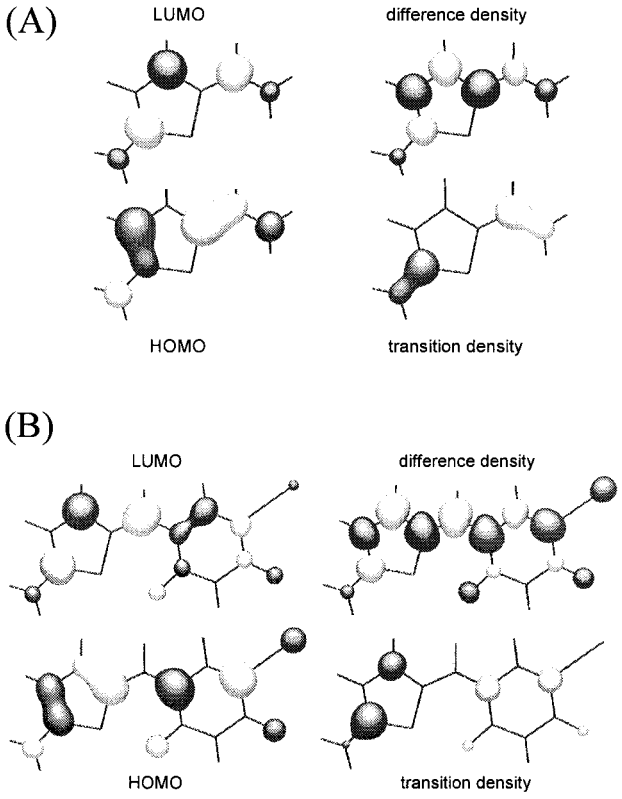

Figure 2. HOMO, LUMO, difference, and transition density for (A) a model cyanine structure with a thiophene core and (B) ATOP dyes calculated with the CNDO/S method for an AM1 optimized geometry (alkyl groups replaced by hydrogen for simplicity).

Scheme 2

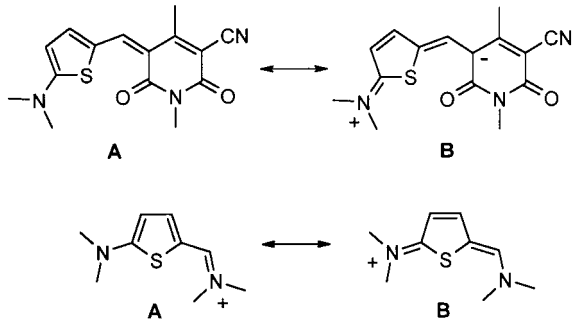

system. Here, the magnitude of the rotational barriers will give valuable information about the orders of the π bonds which have to be broken in the transition state of the internal rotation.

Dynamic NMR spectroscopy is a powerful method for getting insight into the double bond character of C−C and C−N bonds of conjugated compounds.[30] As a prerequisite, the rotational barrier has to be in the energy range accessible by the NMR method (≈20−100 kJ mol^{-1}), and the investigated conformations have to be populated to a detectable amount. In the case of ATOP dyes with identical substituents at the amine, the rotation around the C−N bond is characterized by equal amounts of the two exchanging sites. For the other two possible rotations the situation is more complicated because one conformation is favored over the others (Scheme 3). As shown in Figure 3 (left), cooling of an ATOP-1 solution in $CDCl_3$ causes significant line-broadening of the methylene protons of the amino group (and also the other protons of the alkyl substituents). The coalescence temperature (T_c) is about 255 K. At even lower temperature, separated signals appear which imply a frozen rotation around

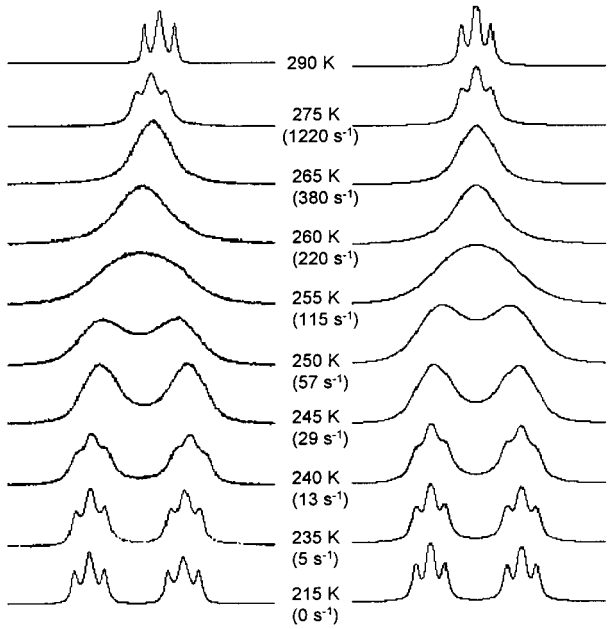

Figure 3. Measured (left, in $CDCl_3$ at the given temperature) and calculated (right, rate constant given) 500 MHz ^{1}H NMR spectra of the AA′BB′ spin system of the $(RCH_2)_2N$ group of ATOP-1.

Scheme 3

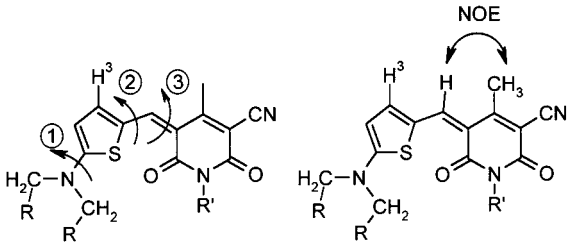

the C−N bond. Total line shape analyses[30,31] were carried out for each temperature to give the respective first-order rate constants and the calculated spectra are shown on the right side of Figure 3. A quantitative evaluation may be done on the basis of Eyring's equation,

$$k = \frac{k_B T}{h} \exp[-(\Delta H^{\neq} - T\Delta S^{\neq})/RT] \qquad (7)$$

where k is the rate constant, k_B Boltzmann's constant, T the temperature, h Planck's constant, and R the molar gas constant. The activation parameters were determined by linear regression of $\log(k/T)$ vs $1/T$ to be $\Delta G^{\neq}(255\ \mathrm{K}) = 52.2$ kJ mol^{-1}, $\Delta H^{\neq}(255\ \mathrm{K}) = 72.2$ kJ mol^{-1}, and $\Delta S^{\neq}(255\ \mathrm{K}) = 78.5$ J K^{-1}·mol^{-1}. It is generally accepted that $\Delta S^{\neq}$ and $\Delta H^{\neq}$ values obtained by this procedure are susceptible to considerable errors while the free energies of activation $\Delta G^{\neq}$ are very reliable. Thus, we compare only the $\Delta G^{\neq}$ value for the C−N rotational barrier of ATOP-1 to those of other conjugated amines (Table 2).[32] According to Table 2 the rotational barrier of the C−N bond of ATOP-1 is very similar to the respective bond of penta-

Table 2. Gibbs Free Activation Energies $\Delta G^{\ddagger}$ of ATOP-1 and **12a**−**c**[32a] in $CDCl_3$ at the Coalescence Temperature T_c

	T_c (K)	$\Delta G^{\ddagger}$ (kJ mol^{-1})
ATOP-1	255	52.2[a]
12a	388	81.7[b]
12b	306	61.6
12c	253	51.5

[a] The value at 298 K is calculated to be 49.0 kJ mol^{-1}. [b] For DMF values between 80 and 92 kJ mol^{-1} are reported by several authors using different solvents and different evaluation methods.[30a−c]

Scheme 4

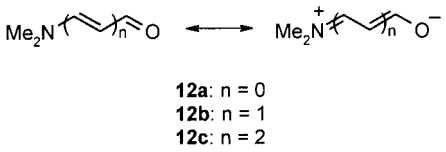

12a: n = 0
12b: n = 1
12c: n = 2

methine **12c** whose C−N π bond order was calculated to be 0.63,[33] close to the cyanine limit of 0.5. Since identical C−N rotational barriers suggest similar CT properties, this result can be viewed as further evidence for the cyanine-like character of ATOP. Obviously, the higher acceptor strength of the pyridone acceptor in ATOP as compared to the aldehyde acceptor unit in **12c** compensates for the counteracting resonance energy of the heterocyclic thiophene core.

Whereas rotation 1 in Scheme 3 could be easily studied by temperature-dependent ^{1}H NMR based on identical populations of the exchanging sites, distinct conformational preferences prevented a comparable study for the other two possible rotations. Strong nuclear Overhauser (NOE) effects between the methine hydrogen and the pyridone CH_3 group suggest the predominance of the structure depicted in Scheme 3, which is also the structure of lowest energy according to AM1 calculations (gas phase).[29] These calculations reveal that steric repulsions between the pyridone CH_3 group and the thiophene core prevent the formation of another planar conformer by rotation 3. On the other hand, considerable line broadening of the ^{1}H resonance of the thiophene proton H3 at higher temperatures (the temperature of maximal line broadening is ca. 315 K in $CDCl_3$) demonstrates a dynamic influence of a slightly populated (<2%) second conformer and allows the estimation of the free energy of activation $\Delta G^{\neq}$ of rotation 2 to be at least 60 kJ mol^{-1}. The existence of such slightly populated conformations in solution as well as the bent shape of the ATOP core may contribute to the high solubility of these dyes (in particular ATOP-4, see Table 4) and also to the excellent morphological stability of PR composites discussed below.

(c) X-ray Crystallography. Final proof for the cyanine-type highly conjugated system and the lowest energy conformation was disclosed by the precise determination of the geometry of ATOP-10 in a single crystal. The ORTEP view shown in Figure 4 reveals an essentially coplanar π-conjugated system with a twisting angle of only 7° between the mean planes of the thiophene and the pyridone rings. This high degree of planarity is accompanied by an expansion of the bond angle of the central methine sp^2 carbon to 137° and a reduction of the S1−O2 distance to 2.58 Å, which is significantly less than the sum of the van der Waals radii (3.25 Å). The optical and electronic properties of the ATOP chromophore are mainly reflected by the bond distances along the conjugated path N1−C1−C2−

(31) (a) Binsch, G.; Kessler, H. *Angew. Chem.* **1980**, *92*, 445−463; *Angew. Chem., Int. Ed. Engl.* **1980**, *19*, 411. (b) Feigel, M. *J. Phys. Chem.* **1983**, *87*, 3054−3058.

(32) (a) Radeglia, R. *Z. Phys. Chem. (Leipzig)* **1967**, *235*, 335−339. (b) Blanchard, M. L.; Chevallier, A.; Martin, G. J. *Tetrahedron Lett.* **1967**, *50*, 5057−5060. (c) Filleux-Blanchard, M. L.; Clesse, F.; Bignebat, J.; Martin, G. J. *Tetrahedron Lett.* **1969**, 981−988. (d) Kramer, H. E. A.; Gompper, R. *Z. Phys. Chem. Neue Folge* **1964**, *43*, 292−303. (e) Wiberg, K. B.; Rablen, P. R.; Rush, D. J.; Keith, T. A. *J. Am. Chem. Soc.* **1995**, *117*, 4261−4270.

(33) Leupold, D.; Dähne, S. *Theor. Chim. Acta* **1965**, *3*, 1.

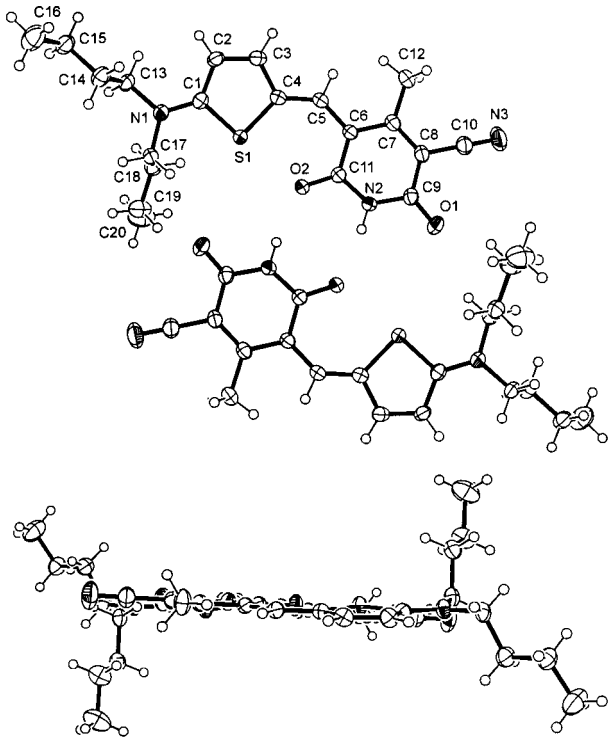

Figure 4. ORTEP drawings for ATOP-10 in the crystal showing the dimeric unit of two ATOP-10 molecules connected by hydrogen bonding in an antiparallel fashion (top view and side view).

Table 3. Selected Bond Distances for ATOP-10 in the Crystal (Å)[a]

atom 1	atom 2	*L*	atom 1	atom 2	*L*
C13	N1	1.469 (2)	C6	C7	1.427 (3)
C17	N1	1.470 (2)	C7	C8	1.380 (3)
N1	C1	1.334 (3)	C8	C9	1.447 (3)
S1	C1	1.744 (2)	C8	C10	1.428 (3)
S1	C4	1.769 (2)	C10	N3	1.150 (3)
C1	C2	1.417 (3)	C9	O1	1.229 (2)
C2	C3	1.356 (3)	N2	C9	1.380 (2)
C3	C4	1.420 (3)	C11	N2	1.377 (2)
C4	C5	1.375 (3)	C6	C11	1.442 (3)
C5	C6	1.417 (3)	O2	C11	1.243 (2)

C3−C4−C5−C6−C7−C8−C9/C10 (Table 3), which reveal almost equal bond lengths as expected for a cyanine-type chromophore in accordance with the canonical structures given in Scheme 2. For the thiophene ring we even note a higher contribution of the quinonoid[34] compared to the aromatic[35] structure, i.e., the shorter carbon−carbon distance is observed for the $C_\beta-C_\beta$ bond and the longer distances are given for the $C_\alpha-C_\beta$ bonds (Table 3). Furthermore, the N1−C1 bond is among the shortest bonds known between an amine and an aromatic carbon and the methine bridge is almost symmetrical with the shorter bond between the C4 and C5 carbon atoms. This indicates that highly polar surroundings such as the bulk solid-state polarize the ATOP chromophore toward a more zwitterionic conjugated system.

With regard to the morphological properties discussed in the second part of the paper some comments on the packing of ATOP-10 in the crystalline state are of interest. Thus the dimeric unit depicted in Figure 4 contains two ATOP dyes linked together by two hydrogen bonds between the imide groups at a distance of 2.87 Å for O2···N2′ and N2···O2′, respectively. This arrangement leads to a densely packed centrosymmetric unit, which exhibits an antiparallel orientation of the dipole moments of the two chromophores. Thus, in addition to hydrogen bonding also the dipolar interaction energies are considerably reduced. The space surrounding this dimer consists of a "cocoon" of alkyl groups made up of the dibutylamino substituents of the depicted and the neighboring molecules without any $\pi-\pi$ interactions between the conjugated systems of the individual dye molecules. It is clear that this hydrogen bond-directed arrangement is a unique feature of ATOP-10. If no hydrogen bonding is possible as in the other ATOP dyes, the packing in the solid state will arise from the remaining dipolar and dispersion interactions. Despite considerable efforts none of the other dyes bearing alkyl substituents at the imide group could be grown in crystals of sufficient size suited for X-ray crystallography. Possible reasons for the resistance toward well-ordered dye packing might be given by a high conformational disorder in solution (see the NMR studies above) or the formation of antiparallel dimer aggregates[21] which cannot pack easily in a three-dimensional lattice. Nevertheless, we assume that all ATOP dyes of this study exhibit a perfectly flat π-conjugated core as found for ATOP-10.

To summarize our structural studies, characterization of the molecular properties of the ATOP chromophore by optical, electrooptical, NMR, and crystallographic methods as well as semiempirical calculations revealed a highly delocalized cyanine-type electronic system. In solvents of low polarity (such as dioxane used for the EOA investigation) almost identical contributions of the neutral and the zwitterionic canonical resonance structures (Scheme 2) were observed, yielding a c^2 value of 0.46 characteristic of an almost perfectly balanced polymethine chain. However, more polar environments such as the solid state or the photoconducting PVK (see vide infra) may further polarize the conjugated system and lead to the more zwitterionic PR optimum suggested by eq 1.

Materials Related Properties of ATOP Dyes. The ideal EO chromophore for PR applications has to combine the highest possible electrooptic response with other important properties such as thermal, chemical, and photochemical stability as well as electrical and structural compatibility with the photoconducting polymer. The characterization and optimization of these properties will be discussed in the following sections.

(a) Thermal Behavior of Pure ATOP Dyes. The thermal properties of ATOP dyes were investigated by thermal gravimetric analysis (TGA) and differential scanning calorimetry (DSC). TGA gives information on the thermal stability of a material, whereas DSC provides additional information on melting enthalpies as well as glass formation capabilities.[36] We obtained decomposition temperatures (T_d) of about 220 °C for all ATOP dyes and melting temperatures, T_m, and melting enthalpies, ΔH_m, as detailed in Table 4. A crude correlation between the percentage of the aliphatic part and T_m is observed. The parent chromophore ATOP-5 (all substituents = methyl) exhibits the highest melting point, while ATOP-4 with the highest alkyl content of almost 50 wt % has the lowest T_m.

(34) For crystallographic data on quinonoid dihydrothiophene-2,5-diylidenes see: (a) Takahashi, K.; Suzuki, T.; Akiyama, K.; Ikegami, Y.; Fukazawa, Y. *J. Am. Chem. Soc.* **1991**, *113*, 4576−4583. (b) Hieber, G.; Hanack, M.; Wurst, K.; Strähle, J. *Chem. Ber.* **1991**, *124*, 1597−1605.

(35) For crystallographic data of oligothiophenes see: (a) Bak, B.; Christensen, D.; Hansen-Nygaard, L.; Rastrup-Andersen, J. *J. Mol. Spectrosc.* **1961**, *7*, 58−63. (b) Visser, G. J.; Heeres, G. J.; Wolters, J.; Vos, A. *Acta Crystallogr. Sect. B* **1968**, *24*, 467−473. (c) Van Bolhuis, F.; Wynberg, H.; Havinga, E. E.; Meijer, E. W.; Staring, E. G. J. *Synth. Met.* **1989**, *30*, 381−389.

(36) (a) Würthner, F.; Sens, R.; Etzbach, K.-H.; Seybold, G. *Angew. Chem.* **1999**, *111*, 1753−1757; *Angew. Chem., Int. Ed. Engl.* **1999**, *38*, 1649−1652. (b) Würthner, F.; Yao, S.; Wortmann, R. *J. Inf. Rec.* **2000**, *25*, 69−86.

Table 4. Alkyl Content, Thermal Behavior during a First and a Second Heating/Cooling Cycle in DSC Experiments, and Solubilities in *N*,*N*-Dimethylaniline for ATOP Dyes

	M_{alk}/M_{ges}[a] (%)	T_m (°C)	ΔH_m[b] (J g^{-1})	T_g (2nd heating) (°C)[c]	solubility (g L^{-1})
ATOP-5	15	310	n.s.	n.s.	0.06
ATOP-2	25	249	n.s.	n.s.	0.4
ATOP-10	31	272	n.s.	n.s.	0.02
ATOP-6	33	235	n.s.	n.s.	1.7
ATOP-7	36	182	88	35[d]	8
ATOP-1	40	198	84	—[e]	12
ATOP-3	40	177	81	36[d]	37
ATOP-8	40	155	73	29	13
ATOP-9	40	182	79	27[d]	34
ATOP-4	47	100	57	16	>300

[a] Percentage of the alkyl part of the molecule to the total molecular mass. [b] n.s. = not studied because of decomposition shortly after the melting temperature. [c] After cooling with a rate of 10 K min^{-1}; heating rate 10 K min^{-1}. [d] Only observed after fast cooling. At a cooling rate of 10 K min^{-1} recrystallization takes place during the cooling cycle. [e] Recrystallization at any cooling rate.

Remarkably, the latter was even difficult to isolate as a solid because of its high solubility and vitrification tendency. The significantly lower melting enthalpy of this dye (Table 4) suggests a partly amorphous solid, which could be isolated from an oil only after being cooled for several weeks in the refrigerator. Therefore, it is not surprising that this dye did not recrystallize from the melt in the DSC experiment and that a glass-transition temperature of 16 °C in the second heating cycle indicates the preferred formation of an amorphous material. A similar DSC behavior was observed for ATOP-8 with a higher T_g of 29 °C. At faster cooling rates of >20 K min^{-1} ATOP-3, -7, and -9 also gave glassy solids. However, in contrast to ATOP-4, all other dyes recrystallized in a second heating cycle indicating lower kinetic stability of their amorphous states. The capability of forming amorphous glassy materials from the melt recommend these dyes as promising candidates for PR composites with long-term morphological stability.

(b) Solubility Studies. The stability of amorphous PR composites consisting of ATOP dyes and the photoconductor PVK against crystallization or phase separation is generally controlled by kinetic and thermodynamic factors. In the ideal case phase separation would be not only slowed for kinetic reasons as in existing materials,[3−7] but thermodynamically prevented by an unlimited miscibility of the components. According to London's theory dispersion interactions between different molecules are maximized if they exhibit the same refractive indices.[37] On a similar basis Hildebrand's solubility parameters[38,39] were derived. Both points of view suggest that the highest miscibility as well as solubility is achieved when the components exhibit similar dipole moments and polarizabilities. Large differences in these properties should lead to phase separation as observed for the majority of polymer composites. In our system the ATOP dye has the higher values for both dipolarity as well as polarizability. It seemed therefore reasonable to reduce these values (for the given volume of dye molecule) to get a closer match to PVK by introducing appropriate amounts of less polar and less polarizable alkyl chains.[40]

To probe the polarity of the photoconducting matrix polymer we applied the solvatochromic method,[39] which allows one to determine the polarity of a microenvironment based on a probe dye whose absorption maximum λ_{ag} strongly depends on the polarity of the surrounding matrix. A good choice for our purpose is the dye 5-(dimethylamino)-5′-nitro-2,2′-bithiophene (**13**), which shows a band shift from 466 nm (yellow) in unpolar solvents up to 600 nm (blue) for solvents of high polarity.[41] This band shift was shown to depend mainly on the dielectric properties (dipolarity and polarizability) of the medium. Thus, dye **13** could be used to derive empirical solvent polarity parameters (π^* values)[42] which by definition range from cyclohexane ($\pi^* = 0.0$) to DMSO ($\pi^* = 1.0$).[41,42] Incorporation of a small amount of **13** into pure PVK resulted in $\lambda_{ag} = 542$ nm, corresponding to a π^*-polarity value of 0.90 that indicates a rather high micropolarity of the polymer PVK comparable to the solvent DMF ($\pi^* = 0.88$).[43] As expected, the polarity of the PVK-based composites increases significantly with polar additives as the azo dye DMNPAA (**2**, Chart 1). For 25 wt % DMNPAA the absorption maximum was shifted to $\lambda_{max} = 555$ nm corresponding to a π^* value of 1.03. Addition of ATOP dyes should similarly increase the polarity. Unfortunately, the strong absorption of ATOP at 500−550 nm obscured the absorption band of the probe dye **13**, preventing a detailed analysis of the polarity of ATOP composites.

The knowledge about the microscopic polarity could now be used to test the dyes' solubility properties in a suitable model solvent. For the purposes of this work the natural choice was *N*,*N*-dimethylaniline ($\pi^* = 0.90$), which shows similar structural features as well as the same π^*-polarity value as the PVK polymer. Table 4 summarizes the observed solubilities of the various ATOP dyes in this solvent. As already noted for the melting behavior again a clear correlation between the mass fraction of alkyl groups and the solubility is observed. The solubilities vary over more than 4 orders of magnitude within the given series. A closer inspection of the data in Table 4 reveals that branched alkyl chains at the imide group and a nonsymmetrically substituted dialkylamino unit further improve the solubility. These observations are rationalized by entropic arguments because statistically distributed conformations have to be ordered during the crystallization process. It is noteworthy that ATOP-4 is soluble to such an extent in *N*,*N*-dimethylaniline that highly viscous oils with more than 30 wt % of the dye are stable at room temperature.

(c) Electrochemical Properties. In addition to efficient electrooptical response to the space-charge grating, high-performance PR materials should have high charge carrier mobilities. Typically this property is provided by photoconducting systems consisting of a photosensitizer and a CTA, which upon illumination form mobile charges localized on radical cationic species. Investigation of the redox behavior of ATOP-1 by cyclic voltammetry in dichloromethane revealed the reversible formation of radical cations at $E = +0.50$ V (vs Fc/Fc$^+$) and no reduction in the accessible potential range (up to -2 V vs Fc/Fc$^+$). For comparison PVK or 9-ethylcarbazole (ECZ) are oxidized at about 0.77 V (vs Fc/Fc$^+$) in a chemically

(37) Israelachvili, J. N. *Intermolecular and Surface Forces*, 2nd ed.; Academic Press: London, 1991; p 102.

(38) (a) Small, P. A. *J. Appl. Chem.* **1953**, *3*, 71−80. (b) Kumar, R.; Prausnitz, J. M. *Solutions and Solubilities, Part 1*; Dack, M. R. J., Ed.; Wiley-Interscience: New York, 1975; pp 259−326.

(39) Reichardt, C. *Solvents and Solvent Effects in Organic Chemistry*, 2nd ed.; VCH: Weinheim, 1990; pp 191−194.

(40) The refractive index of saturated alkanes is roughly 1.4 and thus much smaller than the refractive index of PVK based organic PR materials (1.7).

(41) (a) Effenberger, F.; Würthner, F. *Angew. Chem.* **1993**, *105*, 742−744; *Angew. Chem., Int. Ed. Engl.* **1993**, *32*, 719−721. (b) Effenberger, F.; Würthner, F.; Steybe, F. *J. Org. Chem.* **1995**, *60*, 2082−2091.

(42) Kamlet, M. J.; Abboud, J.-L. M.; Abraham, M. H.; Taft, R. W. *J. Org. Chem.* **1983**, *48*, 2877−2887.

(43) Mecher, E.; Bräuchle, C.; Hörhold, H. H.; Hummelen, J. C.; Meerholz, K. *Phys. Chem. Chem. Phys.* **1999**, *2*, 1749−1756.

Table 5. Compositions of the Investigated Composites

ρ_{DYE} [a]	PVK	ECZ	DPP	TNFM
10	47	21	21	1
20	41	19	19	1
30	37	16	16	1
40	31	14 (20[b])	14 (0[b])	1
50	25	12 (9[b])	12 (9[b])	1

[a] Content of ATOP dye in wt % [b] For ATOP-4 composites.

irreversible process. Thus, the ATOP chromophore is more easily oxidized than the designated carbazole photoconductor, suggesting that the ATOP molecules will act as hole traps in the carbazole photoconducting manifold or might even perform charge transport themselves (see below).

Electrooptical and Photorefractive Properties. (a) Presentation of the Studied Composites. In the following, we will investigate PR composites with the chromophores ATOP-1, ATOP-3, and ATOP-4 as electrooptically active components. The latter were clearly identified as the most promising chromophores on the basis of the solubility/compatibility study presented in the preceding sections (Table 4). The other components in the composites were the photoconducting polymer poly(*N*-vinylcarbazole) (PVK), the plasticizers *N*-ethylcarbazole (ECZ) and diphenylphthalate (DPP), and the photosensitizer 2,4,7-trinitro-9-fluorenylidene-malononitrile (TNFM). TNFM is commonly used for operating wavelengths in the near-infrared.[6,7]

During the preparation of the various composites we discovered that some (those with higher ATOP contents ρ_{DYE} in particular) showed a decrease in PR performance when they were heated above 170 °C in air. By contrast, heating sealed devices even to 190 °C did not lead to degradation. These findings indicate that ATOP dyes decompose by oxidation at elevated temperature in the presence of oxygen. To accomplish processing under ambient conditions at lower temperatures (<160 °C), the plasticizer content was chosen somewhat higher than in previous work.[7] The ATOP content (ρ_{DYE}) was varied between 10 and 50 wt % (Table 5); composites with higher loading (e.g. >75 wt %) could not be prepared due to phase separation of the components. The same composition was chosen for all ATOP dyes except for ATOP-4 where lower amounts of plasticizer had to be added to obtain similar T_g values than for the other dyes. Nevertheless, for a given chromophore content, the resulting T_g's exhibit some variations, e.g. 14 °C for ATOP-1 and ATOP-3 composites and 8 °C for ATOP-4 composites containing 40 wt % of the dye (for the T_g's of the other composites see the Supporting Information).

(b) Absorption Spectra. The absorption spectra were very similar for all composites: a maximum absorption peak was observed at ca. 550 nm, and a shoulder (for low ATOP loading) or a second smaller peak (for high ATOP loading) appeared at about 515 nm (Figure 5). In addition, as reported earlier for ATOP-1,[7b] an increase of ρ_{DYE} led to a sublinear increase of the total absorbance. Both effects could be interpreted in terms of dye aggregation driven by strong dipolar interactions between the dye molecules,[7b] and dimer aggregates consisting of two dye molecules in an antiparallel orientation could be characterized in low-polarity solvents[21] (for spectra and determination of dimerization free energies see the Supporting Information). However, in the rather polar environment of the PVK polymer dimer formation occurs only at rather high concentrations (i.e., in the percent range). From the peak ratios of the monomer and the dimer bands of Figure 5 the amount of aggregated ATOP-4 was estimated to raise from 40% for the composite containing 20 wt % to about 45% for the composite containing 40 wt % dye. In films consisting of pure or 99 wt % ATOP-4 slightly more than 50% of the dye molecules are present as antiparallel dimers.

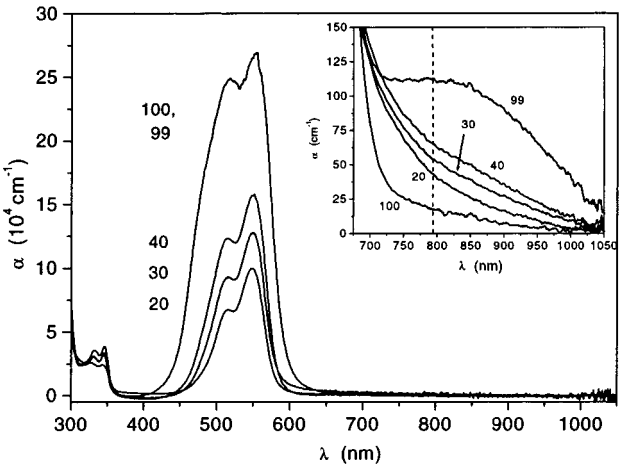

Figure 5. Absorption spectra of PR composites ATOP-4:PVK:ECZ:DPP:TNFM containing different chromophore concentrations ρ_{DYE} (20, 30, 40, 99, and 100 wt %). The main figure shows spectra determined from thin films of about 1 μm thickness (the spectra of $\rho_{DYE} = 99$ and 100 wt % are identical within the experimental resolution); the inset is a more detailed view for the NIR obtained from 37 μm thick PR films. The dashed line indicates the laser wavelength used in the holographic experiments.

The charge-carrier generation efficiency of the PR composite depends on the absorption coefficient at the given laser frequency and the fraction of absorbed photons which are converted into free charges that migrate and form a space-charge field. Composites consisting exclusively of ATOP, PVK, ECZ, and DPP show only weak absorbance at the operating wavelength of the holographic experiments ($\lambda_L = 790$ nm). Addition of a small amount of the sensitizer TNFM, however, leads to substantial absorption at λ_L. In all cases a higher absorption coefficient was observed in the presence of ATOP dyes ($\alpha_{790} = 62-87$ cm^{-1} for the 40 wt % composites)[44] than for carbazole/TNFM ($\alpha_{790} = 14$ cm^{-1}), indicating the formation of charge-transfer (CT) complexes between ATOP dyes and TNFM similar to those reported for 2BNCM (**3**)/TNF[9] and DHADC-MPN (**4**)/TNFM.[6] For the material ATOP-4:TNFM = 99:1 wt % an even larger value of α_{790} (111 cm^{-1}) and a broad CT band are observed (Figure 5). This CT band also could be observed in a UV−vis−NIR titration study where increasing amounts of ATOP-4 were added to a 0.005 M solution of TNFM in dioxane (see the Supporting Information). In view of this intense absorption in the range of operation for common laser diodes and Ti-sapphire lasers (around 800 nm), this complex seems to be well-suited for photosensitization.

(c) Ellipsometry. The efficiency of the ATOP chromophores to transform the molecular FOM into macroscopic refractive index changes Δn was studied by a DC ellipsometric (ELP) technique,[45] which yields information about the field-induced Kerr nonlinearity without complication by the PR space-charge field. A typical data set is displayed in Figure 6. Due to the field-induced changes of the refractive index $\Delta n' = n_P - n_S$, the transmission T_{ELP} shows an oscillatory behavior ($\sin^2$ dependency; see eq 8 in the Experimental Section). For

(44) The α_{790} values for all the other composites are given in the Supporting Information.

(45) (a) Bittner, R.; Meerholz, K.; Bräuchle, C. *Appl. Opt.* **1998**, *37*, 2843−2851. (b) Bittner, R.; Däubler, T.; Neher, D.; Meerholz, K. *Adv. Mater.* **1999**, *11*, 123−128.

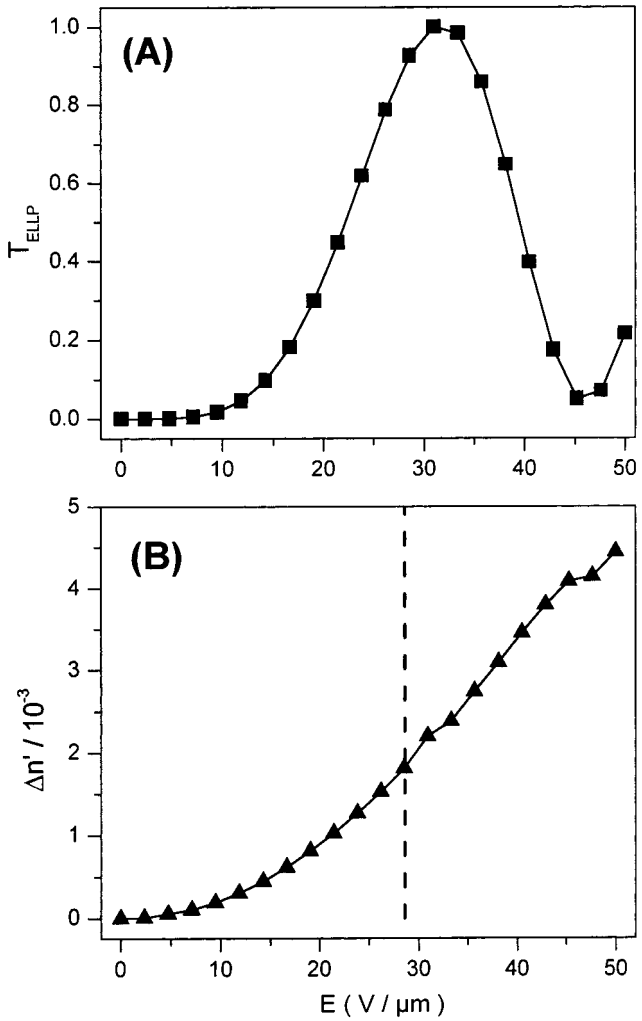

Figure 6. Typical field-dependent data obtained in an ELP experiment: (A) transmission T_{ELP} and (B) field-induced index change $\Delta n'$ calculated with eq 8 for the material containing 40 wt % ATOP-4. The dashed line in part B corresponds to $E = 28.6$ V μm^{-1} at which the $\Delta n'$ data in Figure 7A were determined.

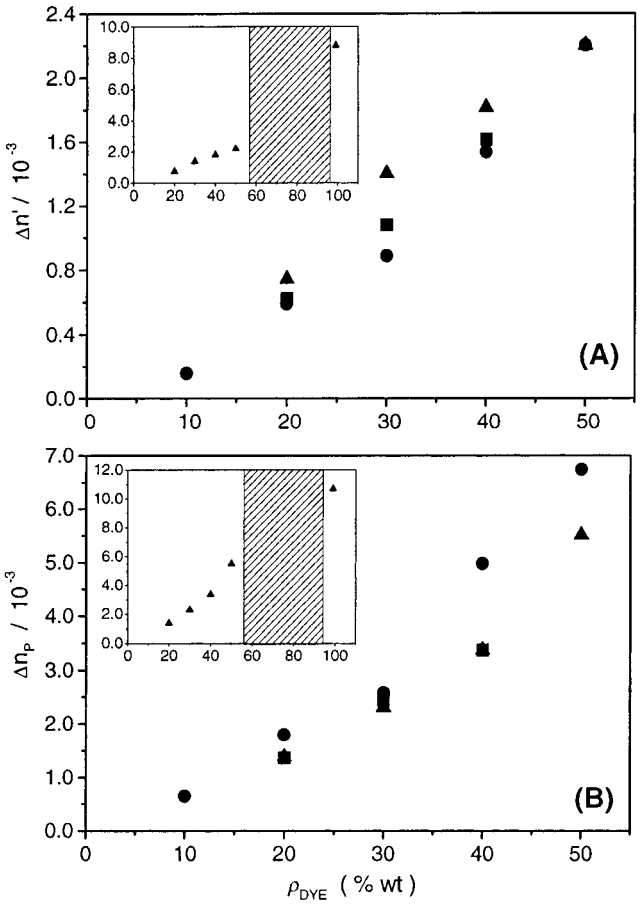

Figure 7. (A) Index change $\Delta n' = n_P - n_S$ calculated from the steady-state transmission in ELP experiments and (B) index modulation for p-polarized readout Δn_P calculated from the steady-state diffraction efficiency in DFWM experiments on PR composites based on the chromophores ATOP-1 (squares), ATOP-3 (circles), and ATOP-4 (triangles) for various chromophore concentrations ρ_{DYE}. Inset: Data for ATOP-4 only. The crossed area qualitatively symbolizes the contents where ATOP-4 is nonmiscible with the PVK matrix. All data apply for $E_{ext} = 28.6$ V μm^{-1}.

comparison of the various materials the field-induced index change $\Delta n'$ was determined for a constant external electric field of $E = 28.6$ V μm^{-1} (Figure 7A). It was found to be very similar for all chromophores and to increase monotonically with ρ_{DYE}. This finding is in contrast to an earlier study where distinct differences occurred between ATOP-1, ATOP-3, and ATOP-4, and an optimum performance for some specific ρ_{DYE} was observed.[7c] Both discrepancies are due to the elevated processing temperatures (temporally >180 °C) used in our earlier study which led to partial decomposition of the chromophore (in particular at higher ρ_{DYE}) and, thus, to a reduced nonlinearity (see also above). In the given study the processing temperature was kept sufficiently low (<160 °C) to avoid such undesired chemical reactions.

Composites based on ATOP-4 yielded the largest $\Delta n'$ for a given ρ_{DYE} possibly due to a ~10 K lower T_g and thus higher orientational mobility in the PVK matrix. The most striking result of the ELP investigations however was that the dependence of $\Delta n'$ on ρ_{DYE} is even slightly superlinear (see the inset in Figure 7A for ATOP-4/TNFM). The so-called "*oriented-gas model*" (OGM), which is well-known from second-order nonlinear optical applications, would predict a linear dependency of $\Delta n'$ on ρ_{DYE} assuming independent chromophores.[46,18a] However, due to dipolar aggregation real systems with large chromophore contents typically show a sublinear dependence of the performance (e.g. of the EO coefficient r_{33}) on ρ_{DYE} or even a performance optimum at intermediate dye contents.[47] A possible explanation for our surprising results (despite dipolar aggregation of ATOP, see above) is that the increase of the matrix polarity at high dye loading ρ_{DYE} reduces the relative amount of aggregated dyes and furthermore polarizes the ATOP chromophore beyond the cyanine limit, which leads to a significant increase of the figure-of-merit F_0^{Kerr}. Indications for such a matrix-assisted enhancement of the EO response were already suggested by the bond-length alternations observed in the crystalline state for ATOP-10, which pointed toward higher c^2 values in more polar surroundings. Nevertheless, the observed $\Delta n'$ of about 0.0015 at $E = 25$ V μm^{-1} (Figure 6B) is still less than expected from the theoretical model[18a] based on independent chromophores which predict $\Delta n' \approx 0.005$ for this field

(46) (a) Singer, K. D.; Sohn, J. E. *Appl. Phys. Lett.* **1986**, *49*, 248−250. (b) Singer, K. D.; Kuzyk, M. G.; Sohn, J. E. *J. Opt. Soc. Am. B* **1987**, *4*, 968−975. (c) Wu J. W. *J. Opt. Soc. Am. B* **1991**, *8*, 142−152.

(47) (a) Dalton, L. R.; Harper, A. W.; Robinson, B. H. *Proc. Natl. Acad. Sci. U.S.A.* **1997**, *94*, 4842−4847. (b) Robinson, B. H.; Dalton, L. R.; Harper, A. W.; Ren, A.; Wang, F.; Zhang, C.; Todorova, G.; Lee, M.; Aniszfeld, R.; Garner, S.; Chen, A.; Steier, W. H.; Houbrecht, S.; Persoons, A.; Ledoux, I.; Zyss, J.; Jen, A. K. Y. *Chem. Phys.* **1999**, *245*, 35−50. (c) Yitzchaik, S.; Di Bella, S.; Lundquist, P. M.; Wong, G. K.; Marks, T. J. *J. Am. Chem. Soc.* **1997**, *119*, 2995−3002.

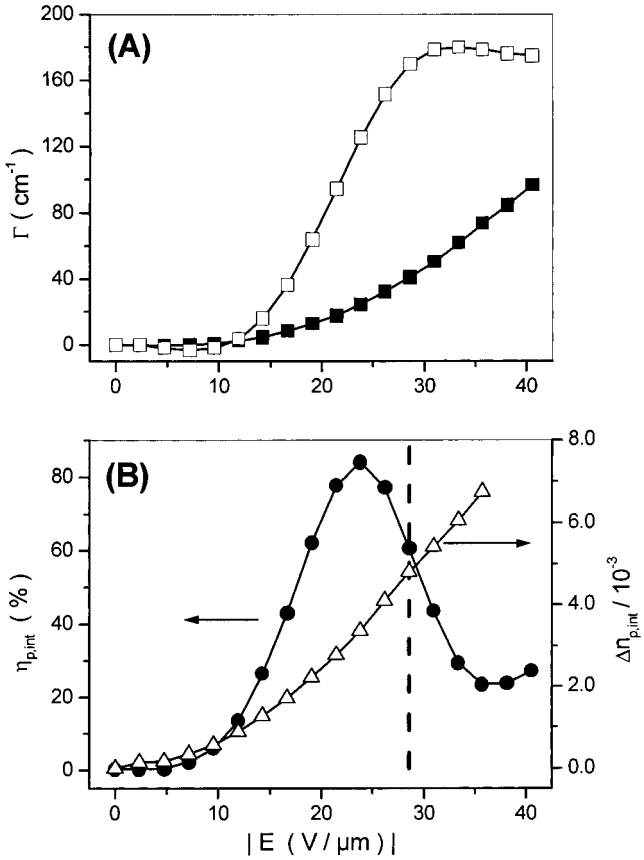

Figure 8. Field-dependent PR performance of the composite containing 40 wt % ATOP-3. (A) Gain coefficients Γ for p-polarized (open squares, $E < 0$) and s-polarized write beams (solid squares, $E > 0$) calculated according to eq 9 (see Experimental Section for details). Note that the external field direction was opposite for the two polarizations. (B) Internal diffraction efficiency for the p-polarized readout of a grating written by s-polarized writing beams calculated according to eq 10 (solid circles) and refractive index modulation Δn_P calculated according to eq 11 (open triangles). The dashed line indicates the field $E = 28.6$ V μm^{-1} for which the Δn_P data in Figure 7B were determined.

strength (estimated on the basis of the dipole moment and polarizability anisotropy of ATOP and using Lorentz local field factors). Accordingly, the observed experimental values are still in the range of our expectations based on the molecular figure-of-merit F_0^{Kerr} and the given aggregation of ATOP dyes at higher concentrations.

(d) Two-Beam Coupling and Degenerate Four-Wave Mixing of Composites. The holographic characterization of PR composites typically involves two-beam coupling (TBC) experiments to prove the PR origin of the recorded gratings[1] and four-wave-mixing (FWM) experiments. The diffraction efficiency η in the FWM experiment depends, besides geometrical factors, mostly on the amplitude Δn of the recorded index grating. By contrast, the energy transfer coefficient Γ ("gain", eq 9, see the Experimental Section) in a TBC experiment is determined by Δn and the phase shift ζ between the light intensity pattern and the recorded index grating.[48] The holographic experiments were performed at a laser wavelength of $\lambda_L = 790$ nm, and the readout in the FWM experiment was performed degenerately at the same wavelength (DFWM; see the Experimental Section for details).

A typical data set is shown in Figure 8 where the gain coefficients Γ_P and Γ_S, the diffraction efficiency η_P, and the index modulation amplitude Δn_P are displayed as a function of the applied electric field E. Similarly to the transmission in an ELP experiment, the diffraction efficiency η_P (defined in eq 10, Experimental Section) shows an oscillatory behavior in agreement with eq 11, which allows calculating Δn_P from η. For comparison of the various composites, Δn_P was determined for a constant external electric field of $E = 28.6$ V μm^{-1} (Figure 7B). Unlike in ELP there are reproducible differences between the different ATOP derivatives, in particular at high dye concentrations. At the moment the origin of these differences remains an open question because several factors are of importance like variations in the T_g values, different aggregation, and dye packing properties, as well as the presence of different numbers of trap sites.[5,49]

Finally, a detailed characterization of the composite containing 40 wt % ATOP-3 was carried out (Figure 8). This material proved to be morphologically stable and exhibits only slightly reduced PR performance compared to the samples containing higher ATOP contents of 50 wt %. In TBC experiments, depending on the polarization of the writing beams, gain coefficients of $\Gamma_P = 50$ cm^{-1} (95 cm^{-1}) and $\Gamma_P = 180$ cm^{-1} at electric fields of $|E| = 30$ (40) V μm^{-1} were observed. For comparison, the absorption coefficient was $\alpha = 62$ cm^{-1}, i.e., net gain was observed for $E > 33$ (18) V μm^{-1} for s (p)-polarized light, respectively. The leveling of Γ_P observed in Figure 8 for $|E| > 30$ V μm^{-1} is related to beam fanning.[50] In the DFWM experiment the maximum of the diffraction efficiency is reached at an electric field as low as $E = 23$ V μm^{-1} for 105 μm thick films. The highest index modulation observed at $E = 40$ V μm^{-1} is $\Delta n_P = 7\times10^{-3}$. This performance compares with PR composites containing the dye DHADC-MPN (**4**), which for identical ρ_{DYE} and field strength exhibited a dynamic range of $\Delta n_P \approx 4.4 \times 10^{-3}$; however, at $\lambda_L = 633$ nm large absorption losses occurred.[6b] At a wavelength more similar to the one we used throughout our studies ($\lambda_L = 830$ nm), the index modulation amplitude of DHADC-MPN composites dropped to only $\Delta n_P \approx 1.5 \times 10^{-3}$ (for $\rho_{DYE} = 0.25$).[6b]

The response time of the grating buildup in DFWM was found to increase with increasing ATOP content. For the lowest ρ_{DYE} (10 wt %) we obtained $\tau_{50} = 0.75$ s for $E = 66.7$ V μm^{-1}, which is slightly slower than the response time of composites containing 50 wt % of the dye DMNPAA (**2**) measured under identical conditions. In all experiments the dynamics of the reorientation of the chromophores as determined by ELP was faster than the holographic response, suggesting that the PR response was not limited by the speed of dye orientation. Therefore, we attribute the observed time constant to the grating formation time, which is slow due to the high polarity of ATOP, its trapping character, and the possible presence of additional deep trapping sites from dimeric species. Since the focus of this work was to improve the dynamic range of the index modulation by optimization of the chromophore, no further studies were performed on the kinetic aspects. Of course, for applications both aspects have to be considered and thus in future work we plan to incorporate ATOP dyes into photoconducting matrices with lower oxidation potentials (e.g. based on the triarylamine photoconducting system). For those materials it is expected that ATOP and ATOP dimers will not act as traps, allowing considerably faster grating formation times.

(48) The exact gain values at high fields depend on the samples' history. Mecher, E.; Meerholz, K. To be submitted for publication.

(49) Grunnet-Jepsen, A.; Wright, D.; Smith, B.; Bratcher, M. S.; DeClue, M. S.; Siegel, J. S.; Moerner, W. E. *Chem. Phys. Lett.* **1998**, *291*, 553−561.

(50) Meerholz, K.; Bittner, R.; De Nardin, Y. *Opt. Commun.* **1998**, *150*, 205−209.

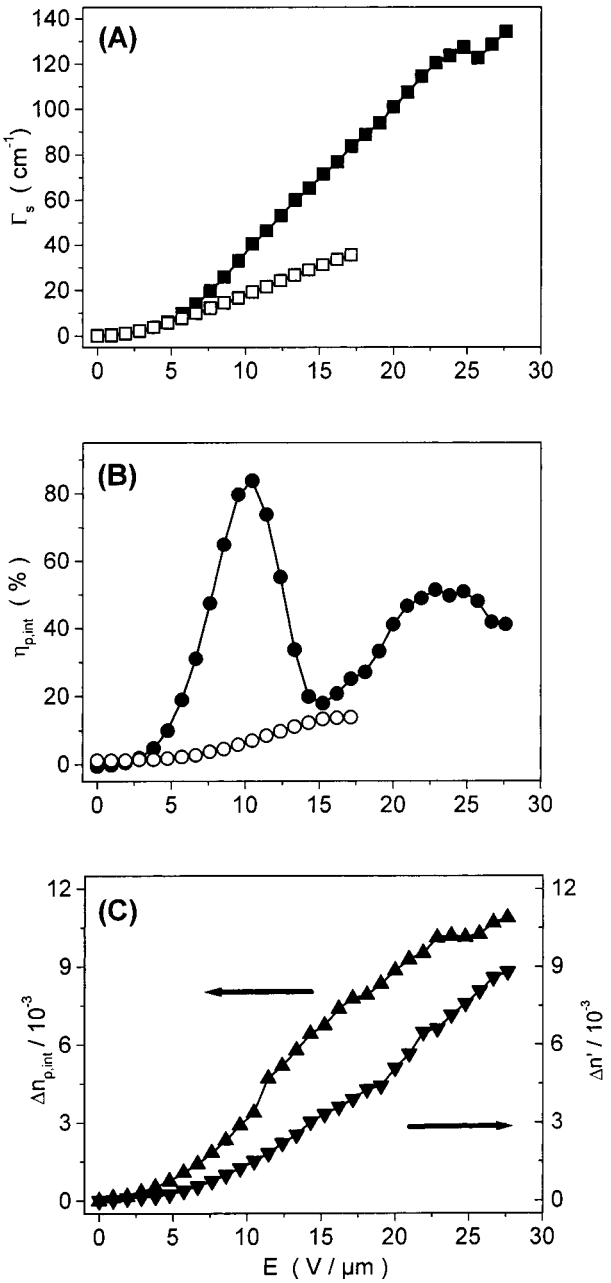

Figure 9. Field-dependence of the steady-state performance of devices containing pure ATOP-4 (open symbols) or ATOP-4/TNFM 99:1 wt % (solid symbols), respectively: (A) gain coefficients in 2BC experiments for s-polarized write beams (squares), (B) internal diffraction efficiency for p-polarized readout of a grating written by s-polarized writing beams calculated according to eq 10 (circles), and (C) refractive index modulation Δn_P in DFWM experiments calculated according to eq 11 (up triangles), and refractive index change $\Delta n'$ in ELP experiments calculated according to eq 8 (down triangles).

(e) TBC and DFWM of ATOP-4 Glasses. The glass-forming properties and the low T_g of ATOP-4 allowed us to prepare PR devices using only the dye without additional sensitizer or hole-conductor. These devices exhibited the PR effect, but only with very limited performance (Figure 9, open symbols). Nevertheless, this experiment demonstrated that ATOP-4 may act as a trifunctional component (EO chromophore, charge generator, and photoconductor).

The steady-state and dynamic PR performance of devices based on ATOP-4 could be strongly enhanced by adding TNFM as a sensitizer (Figure 9, solid symbols). This finding constitutes another unambiguous proof for the formation of CT complexes between ATOP and TNFM, leading to strongly enhanced absorption at 790 nm (increase from 8 to 100 cm^{-1} after addition of TNFM, see Figure 5). Most importantly, this CT complex enables efficient charge generation at the operating wavelength for the ATOP-4:TNFM 99:1 composite. The diffraction maximum in 105 μm thick devices ($\eta_{int} \approx 0.85$, $\eta_{ext} \approx 0.32$) occurred at only 10.5 V μm^{-1}, which is the lowest value ever observed for nonliquid-crystalline organic PR materials up to now. The respective index modulation amplitude and gain coefficient at $E = 28$ V μm^{-1} were $\Delta n_P = 10.7 \times 10^{-3}$ and $\Gamma_P = 130$ cm^{-1}. For comparison, the first multifunctional amorphous low-molar-mass compound 2BNCM (**3** in Chart 1)[9] gave more than 1 order of magnitude smaller index modulation at the same electric field, in agreement with expectations based on the F_0^{Kerr} (=0.30 for 2BNCM[20c]). The only organic PR materials with a comparable dynamic range are polymer-dispersed liquid crystals (PDLC). For PDLCs overmodulation was reported at about 8 V μm^{-1}, and an index modulation amplitude of $\Delta n_P = 3.2 \times 10^{-3}$ was observed at $E = 22$ V μm^{-1} in devices of identical thickness. The diffraction efficiency, however, was limited to about 25%[51] due to scattering of the PDLC droplets.[12c]

Thus, amorphous films from ATOP-4 exhibit about a factor three improvement of the index modulation amplitude over any previous organic PR material at these low electric field values. Comparison of our ELP and DFWM experiments indicates that the ATOP-4 material has even more potential, since $\Delta n_P/\Delta n'$ (i.e., the ratio of the PR index modulation in DFWM compared to field-induced nonlinearity in ELP) is much smaller for $\rho_{DYE} = 0.99$ than for $\rho_{DYE} = 0.50$. As a drawback, amorphous films of ATOP-4 exhibit a rather low resistance to dielectric breakdown, limiting the range of electric fields at this point to $E <$ 28 V μm^{-1}. As a result of these low fields the response time was rather slow (several tens of seconds). In addition, some crystallization occurred within a period of several days, indicating that further chemical modification or addition of small amounts of a binder is needed to obtain a material that is stable against phase separation.

Conclusion

Beginning with the design of a chromophore with an optimized polarizability anisotropy and ending with the characterization of organic thin films of unprecedented PR performance, this paper has described the complete process of the development of a multifunctional material for holographic optical applications. Various experimental techniques were applied during the different stages. Optical and electronic properties on the molecular level combined with stability and morphological issues on the materials level were recognized to be equally important in realizing high-performance bulk functionality.

On the molecular level, a merocyanine dye was designed that exhibits cyanine-type features, i.e., a well-conjugated chain with equal bond orders of 1.5 along the push−pull system, intense and narrow absorption bands, a high polarizability anisotropy, and most importantly a large figure-of-merit F_0^{Kerr}. On the materials level, it was demonstrated that morphological properties such as compatibility, stability, and glass-transition temperature can be controlled by a suitable choice of the functional core which allows derivatization with plasticizing alkyl groups at several positions. This approach bears the distinct

(51) Figure 1 of ref 12c shows an optical loss of 50% at about 8 V μm^{-1}. This corresponds to a loss coefficient of about 130 cm^{-1}, yielding a diffraction efficiency of 0.25 in 105 μm thick devices as used in this study.

advantages of higher volume densities of the functional species and the absence of any phase-separation problems compared to the commonly used approach of incorporating the functional dyes in a matrix of plasticizer and polymer. With regard to the realization of amorphous bulk materials, the comparatively high solubility (considering the strongly dipolar nature of ATOP) and the appreciable thermal stability (for a methine chromophore) are noteworthy properties which seem to be related to the bent, but perfectly planar structure of ATOP.

Owing to the presence of four alkyl substituents given at the ATOP core we could design dyes with high solubilities of more than 300 g L^{-1} in the PVK-like model solvent *N*,*N*-dimethylaniline and a remarkable propensity for the formation of amorphous solid state materials from the melt or casting from solution. For optimized members of this dye family, i.e., ATOP-3 and ATOP-4, long-term morphologically stable PR composites could be prepared which contained up to 50 wt % of the electrooptically active dye in a photoconducting matrix of PVK/ECZ/DPP. Photosensitization at the laser wavelength of 790 nm was accomplished by addition of 1 wt % of the electron acceptor TNFM, which was shown to form a CT complex with PVK as well as with ATOP dyes. The composites were studied by ellipsometric, degenerate four-wave-mixing, and two-beam-coupling techniques. For all investigated ATOP composites a continuous increase of the field-induced birefringence (ELP) and the PR index modulation could be observed with increasing dye content. However, while all composites of a given chromophore content exhibited almost identical performance in ELP, distinct differences were observed in DFWM.

The composite material (ATOP-3:PVK:ECZ:DPP:TNFM 40:31:14:14:1) exhibited an index modulation of $\Delta n_P \approx 7 \times 10^{-3}$ and a gain coefficient of $\Gamma_P = 180$ cm^{-1} at electric fields of only 30 V μm^{-1}. Even higher index modulation efficiencies ($\Delta n_P = 10.7 \times 10^{-3}$ at 28 V μm^{-1}) were observed for films of the pure low-T_g dye ATOP-4 sensitized with 1 wt % TNFM. These experiments proved that ATOP dyes are truly multifunctional π-conjugated systems combining electrooptical, photoconducting, and glass-forming properties. Optimized multifunctional PR systems based on ATOP dyes were demonstrated to exhibit superior index modulation than any other organic PR material including PDLC materials.

Experimental Section

Materials. 2-Brom-5-formylthiophene **7** was prepared according to the literature.[22] 1-Methyl- (**11a**), 1-butyl- (**11b**), 1-hexyl- (**11c**), and 1-(2-ethylhexyl)-4-methyl-2,6-dioxo-1,2,3,6-tetrahydro-pyridine-3-carbonitrile (**11d**) as well as 3-cyano-2,6-dihydroxy-4-methylpyridine (**11f**) were donated by BASF. The characterization of all new compounds was accomplished by ^{1}H NMR spectroscopy (Bruker AM 200 and AM 500), UV/vis spectroscopy (Perkin-Elmer Lambda 40P), and elemental analysis. Melting points were measured with a Büchi SMP-20 and are uncorrected. All dyes used for PR experiments were purified by chromatography and special care was taken to completely remove a violet impurity of lower R_F value (silica; toluene/AcOEt) that was considered to increase the absorption losses of the laser light.

Synthesis. Dialkylaminoformylthiophenes 8a−e (General Procedure):[23] 2-Brom-5-formylthiophene **7**[22] (0.1 mol, 19.1 g), the respective amine (0.3 mol), and *p*-toluenesulfonic acid (0.5 g) were heated at 100 °C for 24 h. The mixture was cooled and 150 mL of water was added. After the mixture was stirred for an additional half hour the product was extracted with CH_2Cl_2. Drying with Na_2SO_4 and evaporation of the solvent gave a dark oil that was chromatographed on silica gel by elution with a 9:1 mixture of toluene/AcOEt to give the dialkylaminothiophenes **8a−e** in 50−70% yield at a purity of >90% which was used for further reactions.

1-Butyl-4-propyl-2,6-dioxo-1,2,3,6-tetrahydro-pyridine-3-carbonitrile (11e): Ethyl cyanoacetate (5.66 g, 0.05 mol) was dropped into *n*-butylamine (4.40 g, 0.06 mol) at 0 °C within 15 min and the mixture was allowed to warm slowly to room temperature and stirred for 12 h to give amide **10b**. Ethyl butyryl acetate (7.91 g, 0.05 mol) and piperidine (5 mL) were added dropwise and the mixture was heated at 100 °C for 20 h. After the mixture was cooled to room temperature the solvent was evaporated, the pH of the residue was adjusted to 1 with 32% aqueous HCl, and the precipitated product was filtered off, washed with water and ether, and dried in vacuo to give 4.61 g of **11e** (purity 98% from NMR, yield 39%). Recrystallization from ethyl acetate gave an analytically pure sample: mp 208 °C; ^{1}H NMR (200 MHz, [D$_6$]DMSO) δ 9.31 (br, 1H), 5.64 (s, 1H), 3.91 (t, $J = 7.4$ Hz, 2H), 2.49 (t, $J = 7.6$ Hz, 2H), 1.56 (m, 4H), 1.28 (m, 2H), 0.91(m, 3H). Anal. Calcd for $C_{13}H_{18}N_2O_2$ (234.3): C, 66.64, H, 7.74, N, 11.96. Found: C, 66.76, H, 7.82, N, 11.96.

1-Alkyl-5-dialkylamino-thiophen-2-ylmethylene-4-alkyl-2,6-dioxo-1,2,5,6-tetrahydro-pyridine-3-carbonitriles (ATOP dyes, general procedure): Equimolar amounts of a dialkylaminothiophenaldehyde **8a−e** and a hydroxypyridone **11a−f** were heated in acetic anhydride (0.5 mL per mmol of **8a−e**) at 90−100 °C for 15−30 min. The deep violet oil was allowed to cool to room temperature with stirring. The slurry formed was diluted with 5−10 mL of 2-propanol and filtered by suction to give a violet solid. After purification all dyes were dried in vacuo at 40−60 °C.

ATOP-1 was synthesized from 3.32 g (12.5 mmol, 90% pure) of **8c** and 2.5 g (12.5 mmol) of **11b**. The crude product was washed with two portions of 5 mL of 2-propanol, purified by chromatography (silica gel, eluent: toluene/AcOEt 7:3), and recrystallized from toluene: 4.27 g (80%) of a red solid, mp 198 °C; ^{1}H NMR (200 MHz, $CDCl_3$) δ 7.53 (s, 1H), 7.51 (d, $J = 5$ Hz, 1H), 6.35 (d, $J = 5$ Hz, 1H), 3.98 (t, $J = 7$ Hz, 2H), 3.53 (t, $J = 8$ Hz, 4H), 2.48 (s, 3H), 1.69 (m$_c$, 6H), 1.40 (m$_c$, 6H), 0.99 (t, $J = 7$ Hz, 6H), 0.93 (t, $J = 7$ Hz, 3H); UV/vis (CH_2Cl_2) λ_{max} nm (ϵ) 538 (150 000). Anal. Calcd for $C_{24}H_{33}N_3O_2S$ (427.6): C, 67.41; H, 7.78; N, 9.83; S, 7.50. Found: C, 67.54; H, 7.67; N, 9.97; S, 7.27.

ATOP-3 was synthesized from 1.2 g (6 mmol, 95% pure) of **8b** and 1.6 g (6 mmol) of **11d** in 5 mL of acetic anhydride. After the product was washed with three 5 mL portions of 2-propanol, 1.8 g of a violet solid was collected and purified by chromatography (toluene/ethyl acetate from 9:1 to 6:4) to give 1.68 g (66%) of green crystals: mp 177 °C, ^{1}H NMR (200 MHz, $CDCl_3$) δ 7.52 (m$_c$, 2H), 6.37 (d, $J = 5$ Hz, 1H), 3.92 (d, $J = 7$ Hz, 2H), 3.62 (q, $J = 7$ Hz, 4H), 2.48 (s, 3H), 1.88 (m$_c$, 1H), 1.37 (t, $J = 7$ Hz, 6H), 1.28 (m$_c$, 8H), 0.89 (m$_c$, 6H). Anal. Calcd for $C_{24}H_{33}N_3O_2S$ (427.6): C, 67.41; H, 7.78; N, 9.83; S, 7.50. Found: C, 67.19; H, 7.65; N, 9.72; S, 7.56.

ATOP-4 was synthesized from 2.4 g (10 mmol) of **8c** and 2.6 g (10 mmol) of **11d** in 6 mL of acetic anhydride. After the product was cooled to room temperature a viscous oil was obtained that solidified during stirring on an ice bath but redissolved on addition of 5 mL of 2-propanol. The mixture was again concentrated to give an oil that was purified by chromatography on silica with toluene/ethyl acetate (9:1 to 7:3) as eluent. After evaporation of the solvent an oil was obtained that started to solidify during stirring on an ice bath. After standing for several days in the refrigerator the product was collected on a Büchner funnel and washed with a little ether and several portions of ether/pentane to give after drying 3.4 g (70%) of a red powder: mp 101 °C; ^{1}H NMR (200 MHz, $CDCl_3$) δ 7.51 (m$_c$, 2H), 6.37 (d, $J = 5$ Hz, 1H), 3.91 (m$_c$, 2H), 3.54 (t, $J = 8$ Hz, 4H), 2.48 (s, 3H), 1.88 (m$_c$, 1H), 1.65−1.82 (m, 4H), 1.28−1.52 (m, 12H), 0.99 (t, $J = 7$ Hz, 6H), 0.90 (t, $J = 7$ Hz, 6H); UV/vis (hexane) λ_{max} nm (ϵ) 531 (115 000); UV/vis (ether) λ_{max} nm (ϵ) 535 (140 000); UV/vis (CCl_4) λ_{max} nm (ϵ) 539 (130 000); UV/vis (MeOH) λ_{max} nm (ϵ) 532 (135 000); UV/vis (CH_2Cl_2) λ_{max} nm (ϵ) 538 (150 000). Anal. Calcd for $C_{28}H_{41}N_3O_2S$ (483.7): C, 69.53; H, 8.54; N, 8.69; S, 6.63. Found: C, 69.26; H, 8.54; N, 8.64; S, 6.89.

Single-Crystal X-ray Structure Determination of ATOP-10. Red prisms of ATOP-10 were obtained from a hot saturated solution in acetic acid by slow cooling to room temperature in a Dewar vessel. The crystals belong to the monoclinic system with cell dimensions $a = 10.9561(9)$ Å, $b = 8.4306(5)$ Å, $c = 21.382(2)$ Å, $\beta = 94.836(11)°$,

and $V = 1967.9(3)$ Å^3. The space group is $P2_1/c$ (IT. No. 14) and $Z = 4$. The empirical formula is $C_{20}H_{25}N_3O_2S$, the molar mass is 371.49, and the calculated density is 1.254 g cm^{-3}. The three-dimensional X-ray data were collected at 220 K by the use of graphite-monochromated Mo Kα radiation ($\lambda = 71.073$ pm) on a Stoe IPDS diffractometer from $2\theta = 3.82-51.94°$. The intensity data of 16401 reflections were collected and 3816 independent reflexes (all with $|F^o| > 4\sigma|F^o|$) were used in the present X-ray analysis. The position of the sulfur atom was located by using the Patterson method of SHELX97 and all non-hydrogen atoms were located and refined by full-matrix least squares against F^2 with use of SHELX97.[52] No absorption correction was performed. Hydrogen atoms were included in the refinement by using a riding model (1.2 times U_{iso} of the attached atom). Block-diagonal least-squares refinements with anisotropic non-hydrogens and isotropic hydrogens have converged to a conventional R-factor of 0.0405 and a weighted R-factor of 0.0975 ($w = 1/[\sigma^2(F_o^2) + (0.0642P)^2)]$, where $P = (F_o^2 + 2F_c^2)/3$.

NMR spectra were recorded on Bruker AM 200 and AM 500 magnetic resonance spectrometers in $CDCl_3$ or [D_6]DMSO, using TMS (0.0 ppm) and [D_5]DMSO (2.49 ppm) as internal standards, respectively. Dynamic NMR investigations were carried out at 500.13 MHz from 215 to 315 K and the temperature was calibrated based on the separation of the highest and the third highest field peaks of the ^{13}C carbons of neat 2-chlorobutane. For the evaluation of the rotational barrier of the N−C bond a series of 7 experiments at temperatures between 235 and 265 K separated by 5 K intervals were used (see Figure 3) and the spectrum at 215 K was taken to define the static parameters of the AA′BB′ spin system. For each temperature the mean lifetime, $\tau = k^{-1}$, was obtained by using the WIN-DYNAMICS software package of Bruker-Franzen, version 1.0, where the computer-generated line shapes are fitted to the experimental line shapes by varying the rate constant k. The activation parameters $\Delta G^{\neq}$, $\Delta H^{\neq}$, and $\Delta S^{\neq}$ were obtained by linear regression analysis of a plot of $\log(k/T)$ against $1/T$ according to the Eyring eq 7 with the transmission coefficient set to 1.

UV/Vis, EOA, and Kerr Effect Studies. UV/vis absorption spectra were recorded on a Perkin-Elmer Lambda 40P instrument at 293 K in Merck Uvasol or Aldrich spectroscopic grade solvents at low concentrations ($<10^{-5}$ mol L^{-1}) with 1 cm cells to determine the absorption maxima λ_{ag} and the molar decadic absorption coefficient ϵ. EOA and Kerr effect measurements were performed with devices described in refs 25, 26, and 53, respectively. The experiments were carried out in the solvent dioxane, which was purified as described in ref 25b and carefully dried by distillation from Na/K in an argon atmosphere prior to use.

Electrochemistry. Cyclic voltammetry was performed with a computer-controlled EG & G PAR 273 potentiostat using a platinum disk (1 mm diameter) working electrode, a platinum wire counter electrode, and a Ag/AgCl wire as the reference electrode that was internally calibrated vs the chemical redox couple of ferrocene/ferrocenium (Fc/Fc^+). The experiments were performed in dichloromethane, which was purified and dried by distillation from CaH_2 prior to use. Tetrabutylammonium hexafluorophosphate (0.1 M) was used as the supporting electrolyte; it was recrystallized twice from methanol/ethanol and dried in vacuo at 100 °C for several days. The dye concentration was in the range of $1-2 \times 10^{-3}$ mol L^{-1}. After the measurement of the sample a small amount of ferrocene was added and an additional cycle was run for internal calibration.

Differential Scanning Calorimetry (DSC). DSC measurements were performed on a Perkin-Elmer DSC 2 or a Mettler Toledo, model 821e. The glass-transition temperatures T_g were determined with 2−3 mg samples by first heating the materials above their melting temperatures (for pure dyes) or 180 °C (for composites) and then cooling the liquid to −50 °C to equilibrate the materials' thermal history. Then another heating−cooling cycle was carried out to determine T_g. The heating rates are given in the text.

Thermal gravimetric analyses (TGA) were carried out with a Perkin-Elmer TGS 2 instrument at a heating rate of 10 K min^{-1} in the temperature range 300−700 K.

Solubility Studies. Concentrated dye solutions in *N,N*-dimethylaniline were prepared by suspending an excess of the respective ATOP dye in 1 mL of *N,N*-dimethylaniline to obtain a saturated solution and subsequent filtering through 0.45 μm filters. The solutions were then diluted and investigated by UV/vis spectroscopy. On the basis of the molar absorption coefficient of 132 000 L mol^{-1} cm^{-1} (determined for three different ATOP dyes for the given solvent), the saturation concentrations given in Table 4 were obtained.

Preparation of Photorefractive Devices. To obtain homogeneous samples all components were taken up in CH_2Cl_2, the solvent was evaporated, and the mixture was softened at temperatures below 160 °C. Devices were prepared by melt-pressing of the composites between two ITO-coated glass substrates with use of glass spacer beads to adjust the film thickness d.

UV/Vis Investigations of the Composites. The absorption coefficients in the near-infrared (NIR) were measured on 37 μm thick glass/composite/glass devices with a Varian Cary 50 spectrometer with a nonabsorbing reference cell. Full spectra were recorded from thin films spin-coated from toluene:cyclohexanone 4:1 solution ($d \approx 1$ μm). The individual thicknesses were determined with a step profilometer (Dectac 4).

Ellipsometry (ELP). To study the poling process independently from the PR grating formation, we determined the changes of the bulk refractive index due to the induced birefringence and the electrooptic effect by a DC ellipsometric (ELP) technique[45] derived from the original work of Teng/Man and Schildkraut.[54] A laser beam (780 nm, 80 mW cm^{-2}) was incident under an external angle of $\theta_{ext} = 60°$ with respect to the sample normal. Its polarization was set to +45°, and the transmitted light was probed through a −45° polarizer. To compensate the phase shift not induced by the polymer, a Soleil-Babinet compensator was placed between the sample and the second polarizer. At zero field the PR material did not affect the polarization state of the probe beam (random orientation of the chromophores) and thus the second polarizer blocked all the transmitted light. With the electric field applied the transmission T through the second polarizer is given by

$$T_{ELP} = \sin^2(C_{ELP} \cdot \Delta n') \tag{8}$$

where $\Delta n' = n_P - n_S$ is the difference between the bulk refractive indices for p- and s-polarization of the incident light, respectively, and $C_{ELP} = [2\pi d \cos(\theta_{int})]/\lambda_L$ is a geometrical constant, d the sample thickness, λ_L the laser wavelength, and θ_{int} the internal angle of the beam relative to the device normal (it was assumed that this angle is identical for s- and p-polarized beams). $\Delta n'$ was calculated from T_{ELP} by using eq 8. The ELP experiments were performed at ambient temperature of 21 ± 2 °C.

Holography. The holographic experiments were carried out at ambient temperature in the typical tilted geometry by overlapping two equally polarized writing beams "1" and "2" from a diode laser (Melles Griot, $\lambda_L = 790$ nm, 28 mW) in devices with thickness $d = 105$ μm. The external angles (intensities) were $\alpha_{1,ext} = 50°$ ($I_{1,ext} = 4.5$ W cm^{-2}) and $\alpha_{2,ext} = 70°$ ($I_{2,ext} = 5.4$ W cm^{-2}). Assuming a refractive index of $n_0 = 1.7$ of the composites yields internal angles of $\alpha_{1,int} = 26.8°$ and $\alpha_{2,int} = 33.6°$. For positive electric fields the positive electrode was facing the writing beams. The field direction is important because of "*beam fanning*"[55] resulting from energy transfer between a laser beam and scattered light. In thin PR samples, this phenomenon leads to coupling of fanned light into the polymer layer and ultimately to a loss of light ($I_1 + I_2 \neq$ constant) by wave-guiding phenomena. As a result unphysical gain values may be obtained.[50,56,57] To avoid this

(52) (a) Sheldrick, G. M.; *SHELXS-97*, Program for the Solution of Crystal Structures, Göttingen, 1997. (b) Sheldrick, G. M.; *SHELXL-97*, Program for the Refinement of Crystal Structures, Göttingen, 1997.

(53) Briegleb, G.; Kuball, H. G. *Z. Phys. Chem. N. F.* **1965**, *45*, 339−345.

(54) Teng, C. C.; Man, H. T. *Appl. Phys. Lett.* **1990**, *56*, 1734−1736. (b) Schildkraut, J. S. *Appl. Opt.* **1990**, *29*, 2839−2941.

(55) (a) Günter, P.; Huignard, J. P. *Photorefractive Materials and their Applications*; Springer: Berlin, 1988 and 1989; Vols. 1 and 2. (b) Yeh, P. *Introduction to Photorefractive Nonlinear Optics*; Wiley: New York, 1993.

(56) Fischer, B.; Segev, M. *Appl. Phys. Lett.* **1989**, *54*, 684−686.

(57) Kokron, D.; Evanko, S.; Hayden, L. M. *Opt. Lett.* **1995**, *20*, 2297−2299.

problem, positive fields ($E > 0$) were used with s-polarized writing beams and negative fields ($E < 0$) with p-polarized beams.[50]

The two-beam coupling (TBC) gain coefficient $\Gamma_{S(P)}$ for s- and p-polarized write beams was calculated from the transmitted write beam intensities I_1 and I_2 according to:

$$\Gamma_{S(P)} = \frac{1}{d}\left[\cos a_{1,\mathrm{int}} \ln\frac{I_1(E \neq 0)}{I_1(E=0)} - \cos a_{2,\mathrm{int}} \ln\frac{I_2(E \neq 0)}{I_2(E=0)}\right] \quad (9)$$

where d is the device thickness (105 μm).

In degenerate four-wave mixing (DFWM) the grating recorded by s-polarized writing beams was read out by a weak ($I_{R,\mathrm{ext}} = 3$ mW/cm^2) p-polarized beam ($\lambda_L = 790$ nm) counter-propagating to write beam "1". The transmitted and diffracted beams were measured by two independent detectors. The internal diffraction efficiency $\eta_{P,\mathrm{int}}$ was calculated according to:

$$\eta_{P,\mathrm{int}} = I_{R,\mathrm{diffr}}/(I_{R,\mathrm{diffr}} + I_{R,\mathrm{transm}}) \quad (10)$$

This definition eliminates the field-dependent absorption and reflection losses and allows a more straightforward evaluation of the data. According to the coupled-wave theory,[58] $\eta_{P,\mathrm{int}}$ can be approximated by:

$$\eta_{P,\mathrm{int}} \approx \sin^2(C_{\mathrm{FWM}}\Delta n_P) \quad (11)$$

where $C_{\mathrm{FWM}} = \pi\, d/[\lambda_L \cos(\alpha_{1,\mathrm{int}})]$ is a geometrical constant and Δn_P the amplitude of the PR index modulation.

All field-dependent steady-state data were obtained by gradually increasing the electric field in steps of 250 V. For each step, the data were taken after this field had been applied for sufficiently long time (typically 2−5 min) to allow the devices to reach quasi-steady-state conditions.

For determination of the response time in DFWM preexisting gratings were erased by illuminating the sample uniformly by write beam "1" for 10 min at zero field. The devices were then poled for 10 min by applying an electric field. During that time, the sample was illuminated by beam "1" only. Finally, write beam "2" was switched on by a magnetic shutter (opening time ≈ 1 ms). Data collection started 10 ms prior to the switching process. The temporal resolution of the setup was 0.5 μs.[59]

Acknowledgment. This work was supported by the VW foundation, the Fonds der Chemischen Industrie and the BMBF (Liebig grant for F.W.), the DFG (Habilitation grant for F.W., research grant Wu 317/1-2 and Graduiertenkolleg "Molecular Organization and Dynamics at Interfaces" at the University of Ulm), the Bavarian government through the program "Neue Materialien", and BASF AG. We thank Prof. P. Bäuerle, Prof. H.-U. Siehl, Dr. G. Höhne, and A. Sautter (all University of Ulm) as well as Prof. C. Bräuchle, R. Bittner, and Y. De Nardin (all University of Munich) for fruitful discussions and their support.

Supporting Information Available: Further experimental details on the synthesis of ATOP dyes, cyclic voltammetry, dimerization studies of ATOP as well as ATOP-TNFM complex formation studies both studied in dilute solution; the glass transition temperatures and absorption coefficients of all PR composites; and the single-crystal X-ray structure determination of ATOP-10 tables of atomic positional parameters, bond distances, bond angles, anisotropic thermal parameters, hydrogen atom positions, and data collection parameters (PDF). This material is available free of charge via the Internet at http://pubs.acs.org.

JA002321G

(58) Kogelnik, H. *Bell Syst. Technol. J.* **1969**, 2909−2947.

(59) Mecher, E.; Bittner, R.; Bräuchle, C.; Meerholz, K. *Synth. Met.* **1999**, *102*, 993−996.